UC Santa Barbara
UC Santa Barbara Previously Published Works

Title
Identification and characterization of deep nitrogen acceptors in β-Ga2O3 using defect spectroscopies

Permalink
https://escholarship.org/uc/item/02m319hq

Journal
APL Materials, 11(11)

ISSN
2166-532X

Authors
Ghadi, Hemant
McGlone, Joe F
Cornuelle, Evan
et al.

Publication Date
2023-11-01

DOI
10.1063/5.0160541

Copyright Information
This work is made available under the terms of a Creative Commons Attribution-NonCommercial-NoDerivatives License, available at https://creativecommons.org/licenses/by-nc-nd/4.0/

Peer reviewed

eScholarship.org Powered by the California Digital Library
University of California

AIP Publishing
APL Materials
ACCEPTED MANUSCRIPT
This is the author's peer reviewed, accepted manuscript. However, the online version of record will be different from this version once it has been copyedited and typeset.
PLEASE CITE THIS ARTICLE AS DOI: 10.1063/5.0160541

Identification and characterization of deep nitrogen acceptors in β-Ga_2O_3 using defect spectroscopies

Hemant Ghadi[1], Joe F. McGlone[1], Evan Cornuelle[1], Alexander Senckowski[2], Shivam Sharma[3], Man Hoi Wong[2], Uttam Singisetti[3], Ymir Kalmann Frodason[4,5], Hartwin Peelaers[6], John L. Lyons[7], Joel B. Varley[8], Chris G. Van de Walle[5], Aaron Arehart[1], Steven A Ringel[1]

[1]Electrical and Computer Engineering, The Ohio State University, Columbus, Ohio, USA
[2]Electrical and Computer Engineering, University of Massachusetts Lowell, Massachusetts, USA
[3]Electrical Engineering, University of Buffalo, Buffalo, New York, USA
[4]Centre for Materials Science and Nanotechnology, University of Oslo, Norway
[5]Materials Department, University of Santa Barbara, California, USA
[6]Department of Physics and Astronomy, University of Kansas, Lawrence, Kansas, USA
[7]Center for Computational Materials Science, Naval Research Laboratory, USA
[8]Lawrence Livermore National Laboratory, San Francisco, California, USA

ABSTRACT:

The ability to achieve highly-resistive beta-phase gallium oxide (β-Ga_2O_3) layers and substrates is critical for β-Ga_2O_3 high voltage and RF devices. To date, the most common approach involves doping with iron (Fe), which generates a moderately deep acceptor-like defect state located at E_C-0.8 eV in the β-Ga_2O_3 bandgap. Recently there has been growing interest in alternative acceptors such as magnesium (Mg) and nitrogen (N) due to their predicted deeper energy levels, which could avoid inadvertent charge modulation during device operation. In this work, a systematic study that makes direct correlations between the introduction of N using ion implantation and the observation of a newly observed deep level at E_C-2.9 eV detected by deep-level optical spectroscopy (DLOS) is presented. The concentration of this state displayed a monotonic dependence with N concentration over a range of implant conditions, as confirmed by secondary ion mass spectrometry (SIMS). With a near 1:1 match in absolute N and E_C-2.9 eV trap concentrations from SIMS and DLOS, respectively, which also matched the measured removal of free electrons from capacitance-voltage studies, this indicates that N contributes a very efficiently incorporated compensating defect. Density functional theory (DFT) calculations confirm the assignment of this state to be an N (0/-1) acceptor with a configuration of N occupying the oxygen site III [$N_{O(III)}$]. The near ideal efficiency for this state to compensate free electrons and its location toward the midgap region of the β-Ga_2O_3 bandgap demonstrates the potential of N doping as a promising approach for producing semi-insulating β-Ga_2O_3.

AIP Publishing APL Materials ACCEPTED MANUSCRIPT
This is the author's peer reviewed, accepted manuscript. However, the online version of record will be different from this version once it has been copyedited and typeset.
PLEASE CITE THIS ARTICLE AS DOI: 10.1063/5.0160541

Beta-phase gallium oxide (β-Ga_2O_3) possesses an ultra-wide bandgap (UWBG) of 4.6-4.8 eV[1–3], inherent n-type conductivity with donor impurities[4,5], and projected high radiation hardness[6,7]. The advantageous material properties of β-Ga_2O_3 lead to outstanding device figures of merit projections that can revolutionize high voltage and RF devices. As a result of these anticipated performance specifications, a large body of research has focused on advancing the quality of gallium oxide materials, heterostructures, and a wide variety of devices. To date, high breakdown β-Ga_2O_3 metal-semiconductor field-effect transistors (MESFETs)[8], high 2DEG charge densities in $(Al_xGa_{1-x})_2O_3$/Ga_2O_3 modulation-doped field-effect transistors (MODFETS)[9], and enhancement mode β-Ga_2O_3 transistors[10] have been epitaxially grown on Fe-doped β-Ga_2O_3 semi-insulating substrates. For these lateral devices, it is necessary to have semi-insulating or highly resistive buffers or substrates acting as a blocking layer to prevent buffer leakage. Regardless of the growth method, the unintentional n-type conductivity can be compensated by introducing deep acceptor-like impurities. Density functional theory (DFT) calculations have identified several impurities that are predicted to form deep acceptor-like bandgap states, such as iron (Fe), nitrogen (N), cobalt (Co), and magnesium (Mg)[11–14]. These deep acceptors can be used as dopants to compensate for excess electrons and create highly resistive layers. Of these, Fe has been adopted in most cases for achieving highly resistive and semi-insulating bulk β-Ga_2O_3 substrates and epitaxial layers[12,15,16].

Due to this popularity, much work has been published regarding the properties of Fe in β-Ga_2O_3. Computational results validated by deep-level (thermal) transient spectroscopy (DLTS), electron paramagnetic resonance (EPR), and cathodoluminescence (CL) experiments have demonstrated that Fe incorporates into n-type β-Ga_2O_3 as an acceptor-like defect.[12,17–26] It is predicted to preferentially substitute on the Ga sites in the β-Ga_2O_3 lattice, creating a bandgap state at E_C-0.8 eV (commonly referred to as E2).[12,27] However, with an activation energy of only 0.8 eV below the conduction band, Fe has shown to be a source of device instabilities. For example, McGlone *et al.* have shown a clear link between the thermal emission of electrons from the E_C-0.8 eV Fe state during device biasing and significant threshold voltage instabilities for β-Ga_2O_3 delta doped MESFETs.[28] This results from Fe incorporation from the Fe-doped substrates tailing into the unintentionally doped (UID) epitaxial buffer layer between the substrate and the 2DEG device channel. Hence, while this degradation mode can be mitigated by using thicker UID buffers [19], this highlights the concern that the E_C-0.8 eV position of Fe acceptors in the 4.6-4.8 eV bandgap of β-Ga_2O_3 may not be ideal since its charge state can be modulated during device biasing and trapped electrons can be thermally emitted. An impurity with a deeper acceptor level could therefore be advantageous in reducing the chance of modulating its charge state during biasing and becoming thermally ionized, even at the high operating temperatures envisioned for β-Ga_2O_3 power electronics.

As a result, there is interest in alternative acceptor-like dopants to Fe. A recent study published by Seyidov *et al*. demonstrated cobalt doping in Czochralski (CZ) growth resulting in semi-insulating β-Ga_2O_3 substrates with the Fermi level pinned at E_C-2.1 eV.[13] Similarly, Mg doping has resulted in high-quality semi-insulating β-Ga_2O_3 materials with a predicted acceptor level at E_C-3.4 eV by DFT.[11,14,29] Nitrogen has been identified as a deep acceptor candidate by Peelaers *et al.* through DFT calculations.[11] N substituting on oxygen I, II, and III sites in the β-

AIP Publishing APL Materials ACCEPTED MANUSCRIPT
This is the author's peer reviewed, accepted manuscript. However, the online version of record will be different from this version once it has been copyedited and typeset.
PLEASE CITE THIS ARTICLE AS DOI: 10.1063/5.0160541

Ga_2O_3 lattice forms acceptor-like levels with (0/-1) charge-state transition levels at E_C-1.61 eV, E_C-1.46 eV and E_C-2.84 eV, respectively.[11] In recent experimental measurements after ion implantation, N was found to diffuse only at temperatures greater than 1100ºC, while Mg diffusion was observed at temperatures as low as 800ºC.[30,31] Using these results and evaluating them with transition state theory, barrier diffusion activation energy of 3.87 eV for N and 2.84 eV for Mg was obtained.[11,30] Large activation energies indicate high thermal stability in extreme environments and are desirable for deep acceptor dopants. In addition, the ion implantation study reported that a high acceptor doping efficiency was achieved using N.[30] Nitrogen has been successfully incorporated in epitaxial layers grown by metal-organic chemical vapor deposition (MOCVD) using an N_2O precursor, resulting in room-temperature electron mobility of 153 cm^2/Vs and low net ionized doping concentration of 10^{14} cm^{-3}.[26,32] With these promising preliminary work as motivation and given the lack of experimental knowledge regarding the nature of nitrogen-related defects within β-Ga_2O_3, we have undertaken a study to investigate the electronic properties associated with nitrogen-related deep-level defects within β-Ga_2O_3. A combination of both deep-level transient (thermal) spectroscopy (DLTS) and deep-level optical spectroscopy (DLOS) measurements were applied to a systematic sample set of Si and N co-doped β-Ga_2O_3 materials designed to allow for precise and quantitative identification of nitrogen-related defect states in β-Ga_2O_3, which were confirmed by DFT calculations. This study suggests very efficient incorporation of nitrogen into a preferred configuration in the β-Ga_2O_3 lattice, having an energy level of E_C-2.9 eV, implying significant promise for future applications of nitrogen doping to create ideal, highly resistive β-Ga_2O_3 materials for implementation into future device technologies.

TEST STRUCTURES

A systematic set of experiments was performed using several N-implant conditions on thick, Si-doped hydride vapor phase epitaxy (HVPE) grown β-Ga_2O_3 materials with (001) orientation to investigate the introduction of deep levels associated with nitrogen. The reference sample was a 10 μm thick Si-doped HVPE grown epilayer on a highly conductive (n = 3-5×10^{18} cm^{-3}) Sn-doped β-Ga_2O_3 substrate procured from Novel Crystal Technology.[33,34] The HVPE-grown epilayer was doped with Si to achieve a net ionized doping concentration of 1.2×10^{17} cm^{-3}. This value was chosen so that subsequent nitrogen co-doping via ion implantation could be used to achieve nitrogen concentrations high enough to be measured using secondary ion mass spectrometry (SIMS), i.e., above the SIMS detection limit of ~ 1×10^{16} cm^{-3}, while simultaneously producing an appropriate degree of carrier compensation to be within ideal measurement conditions for capacitance-based DLTS and DLOS characterization. Using Stopping and Range of Ions in Matter (SRIM) simulations,[35] a uniform implantation profile was created by combining nitrogen implant energies from 10-680 keV, each with different dose; an example of the individual implant profiles is shown in Fig 1a in the light grey curves. The cumulative nitrogen implant profile from the individual energy implants results in the desired uniform nitrogen concentration profiles. Two sets of samples were created, one with a uniform nitrogen doping of 2×10^{16} and another at 5×10^{16} cm^{-3}, within the top ~0.8 μm of the HVPE layer, depicted in Fig 1a. The implantation was performed using a commercial implanter (Cutting Edge Ions). Post-implantation annealing was performed at

ACCEPTED MANUSCRIPT
APL Materials
AIP Publishing
This is the author's peer reviewed, accepted manuscript. However, the online version of record will be different from this version once it has been copyedited and typeset.
PLEASE CITE THIS ARTICLE AS DOI: 10.1063/5.0160541

1100ºC in nitrogen ambient for 10 minutes using a rapid thermal annealing system to remove implantation damage and activate the dopants as reported elsewhere.[30] The annealing was performed on ULVAC technology MILA 3000 rapid thermal annealing (RTA) system.

Multiple Schottky diodes were fabricated on each of the three samples: a baseline HVPE sample without implantation and annealing and the two implanted and annealed samples with nitrogen concentrations of 2×10^{16} and 5×10^{16} cm^{-3} confirmed by SIMS (discussed later). The Schottky diode fabrication process in all cases is now described. All samples were solvent cleaned with acetone and isopropyl alcohol (IPA), followed by a rinse in deionized (DI) water. Semi-transparent 8 nm Ni Schottky contacts (290×290 μm^2) were then deposited using electron (e)-beam evaporation, followed by an e-beam deposited ohmic contact stack of Ti/Al/Ni/Au (20/200/30/200 nm) on the back side of the conducting substrate. A thick Ni/Au (30/200 nm) contact stack of 25×25 μm^2 was deposited on a small area of the thin 8 nm semi-transparent Ni-Schottky for probing the device and making stable contacts during measurements. A cross-sectional diagram depicting the fabricated diodes on the baseline HVPE and the post-implant annealed samples are shown in Fig 1b and c, respectively. The fabricated samples yielded dozens of high-quality Schottky diodes across each sample, with nearly identical I-V characteristics having ideality factors of 1.1 ± 0.05 and leakage current densities below 10^{-9} A/cm^2. Typical Schottky barrier heights were found to be ~ 1.4 V as measured using internal photoemission (IPE) spectroscopy, with negligible changes after N-implantation.[36,37]

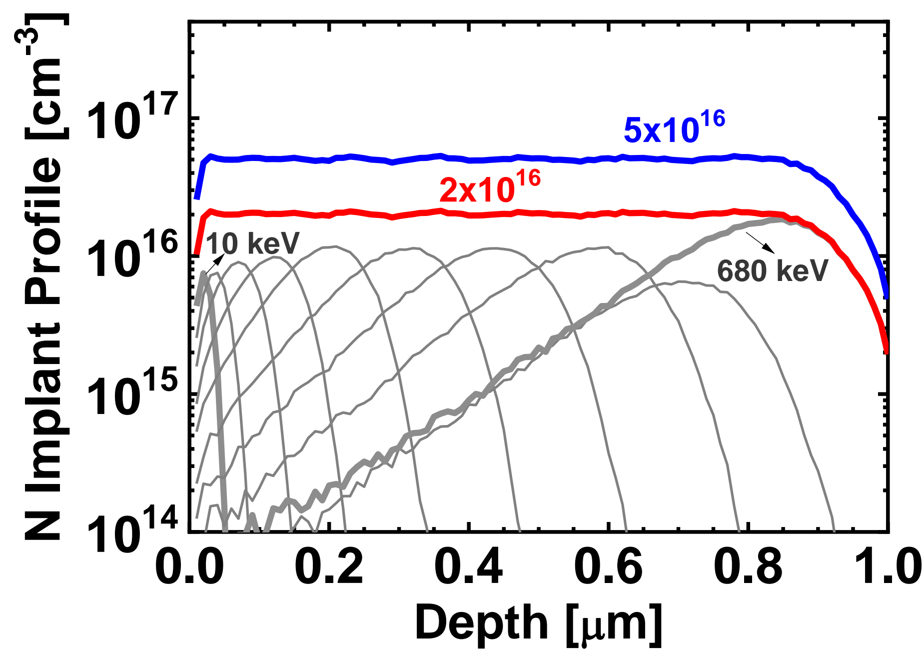

(a)

ACCEPTED MANUSCRIPT
APL Materials
AIP Publishing
This is the author's peer reviewed, accepted manuscript. However, the online version of record will be different from this version once it has been copyedited and typeset.
PLEASE CITE THIS ARTICLE AS DOI: 10.1063/5.0160541

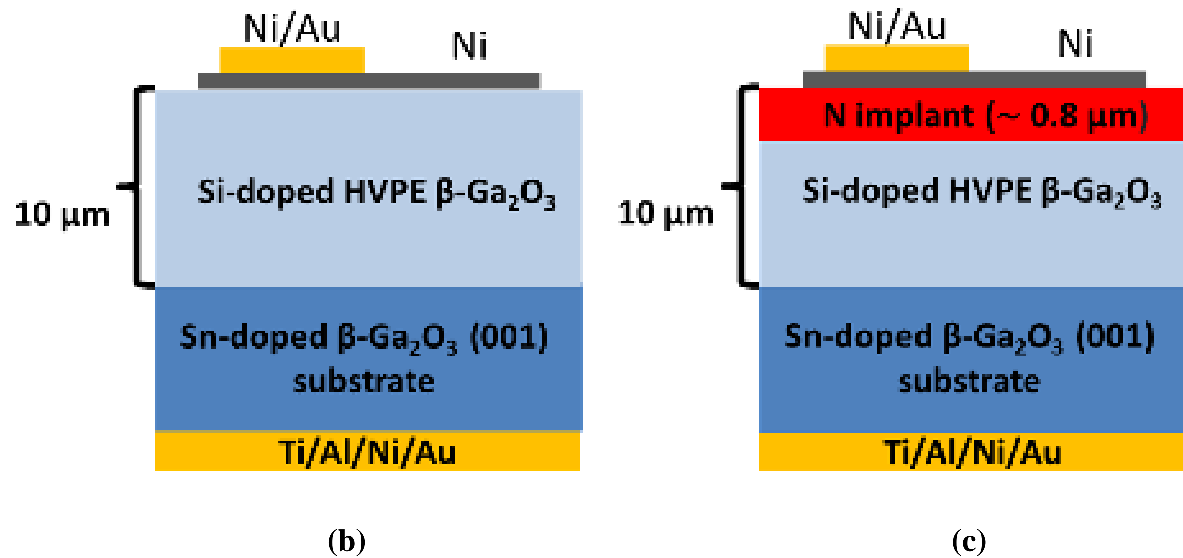

Fig 1: (**a**) Nitrogen implantation profiles simulated using SRIM and implemented by implanting with multiple energies into the Si-doped HVPE layer for the two target concentrations. The figure provides implant profiles of N for the individual implant energies from 10-680 keV used to achieve the uniform implantation profiles. Cross-sectional diagrams of the fabricated diode structures with Ni-Schottky contacts and backside ohmic on (**b**) the baseline Si-doped HVPE sample and (**c**) the N co-doped sample with the implanted region in the upper 0.8 µm are shown.

DEFECT SPECTROSCOPY

DLTS measurements on the fabricated diodes were carried out over a temperature range from 77K-400K, enabling the determination of concentrations and activation energies for trap states within ~ 1 eV of the conduction band. Briefly, the DLTS conditions used here consisted of a "fill pulse" of 0 V for 10 ms to fill traps, followed by a "quiescent state" reverse bias at -2 V for 2 seconds, during which any capacitance transients due to thermally stimulated electron emission from traps are recorded at each temperature from 77 - 400 K in steps of 0.1 K, and subsequently analyzed using a conventional double boxcar method. The full details of the measurement can be found in previous publications.[38–41] The remaining distribution of trap states in the bandgap was obtained using DLOS measurements. DLOS is based on direct photoemission of trapped carriers from states too deep to be seen by thermally stimulated carrier emission measurements like DLTS. The trap-filling in the depletion region is achieved with a fill pulse voltage of 0.7 V for 10 seconds, followed by a thermal settling time of 100 seconds. Trapped carriers, if any, are then optically emitted by a monochromatized light source providing photons with energies between 1.2-5.0 eV, scanning the bandgap in 0.02 eV steps for 300 seconds each, and photocapacitance transients are recorded. These are subsequently analyzed to extract optical cross-sections of any traps present as a function of photon energy. The extracted optical cross-sections are then fitted to the Pässler model, which enables the determination of the equilibrium trap energy level and the Frank-Condon energy (D_{FC}).[42,43] The concentration of each DLOS-detected state is determined from the steady-

AIP Publishing APL Materials ACCEPTED MANUSCRIPT
This is the author's peer reviewed, accepted manuscript. However, the online version of record will be different from this version once it has been copyedited and typeset.
PLEASE CITE THIS ARTICLE AS DOI: 10.1063/5.0160541

state photocapacitance (SSPC) associated with each state. The lighted C-V (LCV) method was also used to assure complete saturation of the SSPC for accurate trap concentration extraction since we have reported that for cases where a defect state possesses a small optical cross-section, SSPC saturation can be difficult.[36,37,44,45]

As noted above, the Si:N co-doping concentrations were chosen to allow correlations between the nitrogen concentration, carrier compensation, and deep-level concentration by being within the measurement limits of both SIMS and DLTS/DLOS. The nitrogen concentration profiles obtained by SIMS for both target concentrations after the post-implant anneals are shown in Fig 2a, revealing uniform implant profiles in close agreement with the targeted design discussed earlier. Capacitance-voltage (C-V) measurements reveal systematically increased carrier compensation (lower net doping) as a function of increased nitrogen doping, as shown in Fig 2b (It should be noted that without post-implant annealing the implanted samples are fully depleted, presumably due to implantation damage). Based on the simple assumption that each nitrogen defect is activated and removes a single conduction band electron, nitrogen doping should remove approximately 17% and 42% of the free electron concentration in the lower and higher nitrogen co-doped samples, respectively, for each N concentration. However, the results indicate that while almost all the implant damage was removed by the post-implant anneal, the slightly higher amount of carrier removal actually observed, at 27% and 67%, respectively, suggests that some damage in the form of additional compensating defects is likely to remain, in addition to the nitrogen acceptors. This work, however, is not focused on anneal optimization. The next section presents comprehensive DLTS and DLOS investigations, which focus on identifying nitrogen-related states but can also reveal residual defect states that could contribute to the slightly higher degree of observed carrier compensation for the implant and anneal conditions used here.

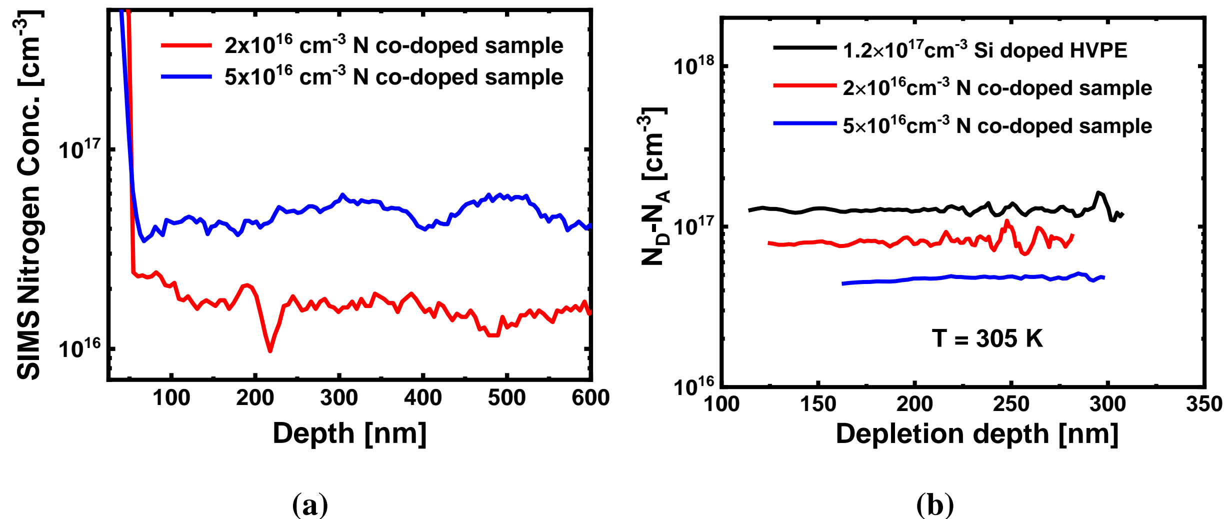

Figure 2: **(a)** The N concentration profiles measured by SIMS in each sample and the **(b)** corresponding net ionized doping (N_D-N_A) concentrations extracted from the CV for each co-doped sample, after both implant and anneal, along with the non-implanted control (black) sample. The N concentration in **(a)** matches the difference in net ionized doping **(b)** between the control

APL Materials ACCEPTED MANUSCRIPT
AIP Publishing
This is the author's peer reviewed, accepted manuscript. However, the online version of record will be different from this version once it has been copyedited and typeset.
PLEASE CITE THIS ARTICLE AS DOI: 10.1063/5.0160541

sample and the respective implanted samples in a monotonic fashion, indicating very efficient carrier removal by N, as desired.

DLTS RESULTS

The DLTS spectra for the baseline and two N co-doped (post-implant and annealed) HVPE samples are shown in Fig 3 a-c, with the Arrhenius characteristic for each DLTS trap shown in Fig 3d. The DLTS spectra reveal states at E_C-0.25 eV, E_C-0.34 eV, E_C-0.4 eV, E_C-0.6 eV, E_C-0.7 eV, and E_C-0.8 eV. The levels at E_C-0.7 eV and E_C-0.8 eV are also present in the baseline Si-doped HVPE sample, while the other four levels were only observed in the N co-doped samples. The trap concentrations for each state were calculated using the "lambda" correction to account for the volume of the depletion region in which the occupancy of the specific trap level is modulated by the DLTS biasing.[40] This is critical for the most accurate concentration values, shown for each trap in Fig 3 a-c.

Several observations are important from the DLTS data. First, none of these energy levels match anywhere close to the predicted nitrogen states previously reported for β-Ga_2O_3. So, the sources of these states are likely due to pre-existing defects in the baseline Si-doped HVPE material or result from implantation damage that was not fully removed by the post-implant anneal process used here and is not related to nitrogen.[7,12,21,46] Second, regardless of their source, the individual and total concentrations of DLTS-detected traps are on the order of 10^{13}-10^{14} cm^{-3}. This is far lower than what can account for the large carrier removal observed in the C-V data. Still, the total is large enough to account for some of the differences between the anticipated and measured amount of carrier removal discussed above. While this work is not focused on optimizing the implant and annealing conditions for nitrogen doping by implantation, it is still helpful to consider possible sources for these defect states to provide insights into the HVPE material and the implant process used here.

To that end, we have included other sets of well-known and commonly observed DLTS data with the Arrhenius plot shown in Fig. 3d, which are associated with Fe impurities and point defects due to high-energy particle irradiation, as labeled in the same figure. Comparisons with the data here are revealing. First, the radiation-induced defect data closely matches three trap states observed here, at E_C-0.34, E_C-0.6, and E_C-0.7 eV.[7,47] Since the proton radiation damage produces intrinsic point defects, these are all likely due to residual damage from the nitrogen implantation process. The state at E_C-0.7 eV has received significant focus in prior work and has been connected with gallium vacancies; recent work has proposed the Ga-O divacancy as the most likely origin.[7,12,17,47] Additionally, the state detected at the E_C-0.8 eV closely matches the well-known trap associated with Fe_{Ga} defects, suggesting that residual Fe is present in the HVPE material.[12,15,21] As noted above, both the E_C-0.7 and E_C-0.8 eV traps are present in the control baseline HVPE sample, and the concentration of the E_C-0.8 eV trap did not change, consistent with its source being residual Fe. Finally, the sources of the remaining two DLTS states at E_C-0.25 eV and E_C-0.4 eV could be introduced by the implant damage and/or by the annealing process. Regardless, none of the DLTS traps have high enough concentrations of consequence to explain the strong carrier compensation observed in the co-doped samples. Thus, the next section focuses on the rest of the bandgap using DLOS measurements.

ACCEPTED MANUSCRIPT
APL Materials
AIP Publishing
This is the author's peer reviewed, accepted manuscript. However, the online version of record will be different from this version once it has been copyedited and typeset.
PLEASE CITE THIS ARTICLE AS DOI: 10.1063/5.0160541

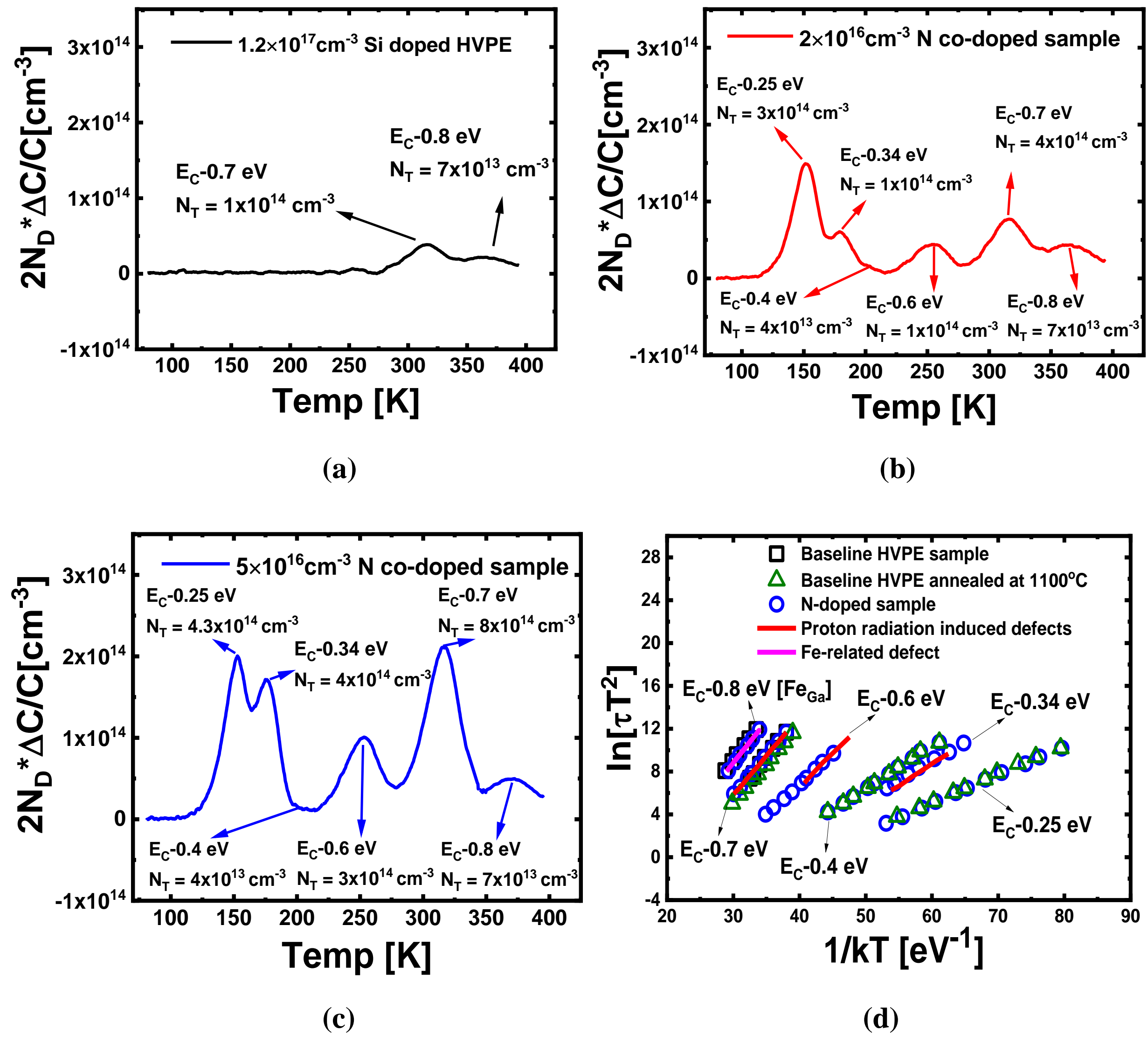

Figure 3: DLTS spectra measured at a rate window of 0.8 s^{-1} on the **(a)** baseline HVPE sample, **(b)** 2×10^{16} cm^{-3} N co-doped sample, and **(c)** 5×10^{16} cm^{-3} N co-doped sample, with lambda corrected concentrations for each state presented in the trap labels. The Arrhenius plot in **(d)** compares the traps from **(a)** – **(c)** with previously published results of traps due to high energy proton irradiation damage and from Fe impurities in β-Ga_2O_3.[7,12,21]

DLOS RESULTS

The individual DLTS measured trap concentrations (~ 10^{13}-10^{14} cm^{-3}) were several orders of magnitude lower than the targeted N concentrations shown in Fig 1a or the measured carrier compensation in Fig 2b. Furthermore, the N on oxygen substitutional sites in β-Ga_2O_3 form acceptor levels predicted by DFT to be significantly deeper than anything observed by DLTS. Therefore, DLOS and LCV measurements were used to interrogate the rest of the bandgap to

AIP Publishing APL Materials ACCEPTED MANUSCRIPT
This is the author's peer reviewed, accepted manuscript. However, the online version of record will be different from this version once it has been copyedited and typeset.
PLEASE CITE THIS ARTICLE AS DOI: 10.1063/5.0160541

investigate the possible presence of other state(s) responsible for the carrier compensation. The SSPC data in Fig 4a reveals three SSPC onsets, at E_C-2.0 eV, E_C-2.9 eV, and E_C-4.4 eV, associated with very deep levels in the bandgap. The concentrations from the SSPC onsets indicate trap concentrations on the order of 10^{16} cm^{-3}, far higher than the DLTS trap concentrations. In order to ensure complete saturation of the DLOS-detected states to compare concentrations with SIMS, LCV measurements were applied to each state. Considering the E_C-2.9 eV state first, Fig. 4b compares independently measured E_C-2.9 eV trap concentrations with SIMS-measured N concentration as a function of the targeted N implant concentration. There is a clear correlation and quantitative match between the concentration of this trap and the total N concentration. The LCV measured trap concentrations for the E_C-2.9 eV state were found to be 1.8×10^{16} cm^{-3} and 4.5×10^{16} cm^{-3} for the 2×10^{16} cm^{-3} and 5×10^{16} cm^{-3} N co-doped samples.

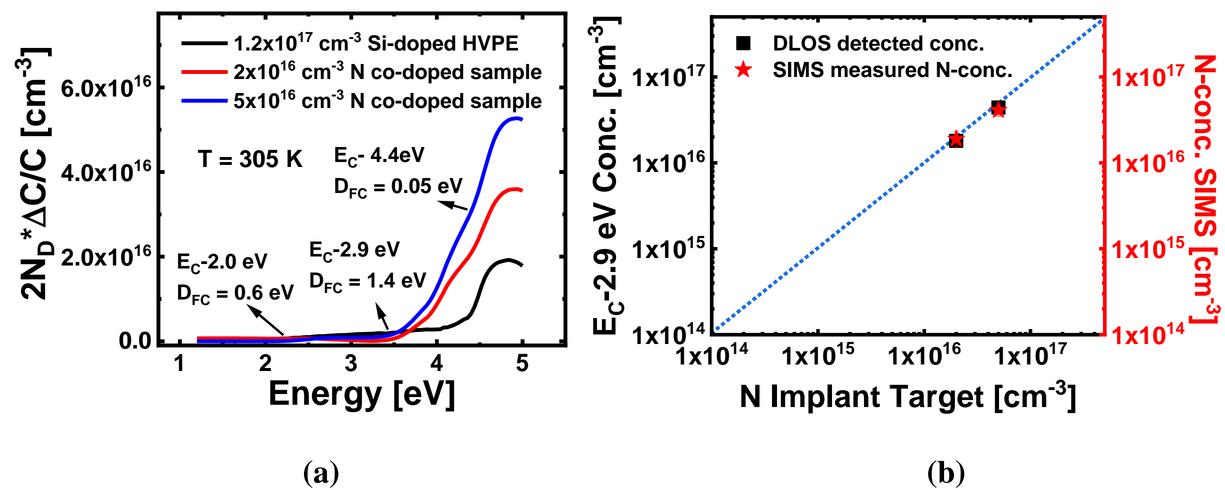

Figure 4(a): Steady state photocapacitance spectra measured on the baseline HVPE and N co-doped samples with the precise trap energy and D_{FC} calculated from optical cross-section fitting to the Pässler model.[43] A monotonic increase in the trap concentration of E_C-2.9 eV state with N is evident from the SSPC spectra. **(b)** This figure shows the match between the E_C-2.9 eV trap concentration measured by LCV, the total N content from SIMS, and the target N implant concentration. The dotted line represents a one-to-one correspondence between the target N concentration and the measured concentrations of N and E_C-2.9 eV trap.

The overall quantitative trends for all detected states as a function of N implant concentrations are depicted in Fig 5, confirming that the primary influence of N doping is on the E_C-2.9 eV state. Before considering the physical defect configuration associated with the E_C-2.9 eV state, the two DLOS detected states at E_C-2.0 eV and E_C-4.4 eV warrant some discussion since both display small but measurable increases in their concentrations with nitrogen implantation, as seen in Fig 5. Previous work on gallium oxide subjected to high energy particle irradiation by both protons and neutrons has connected the E_C-2.0 eV state with a $2V_{Ga}^{1} - Ga_{i}$ defect "split-vacancy" complex,[48] and gallium vacancies will likely form due to the implantation damage (though largely annealed out). The commonly reported E_C-4.4. eV state is not well understood, and its physical source is still being explored, with prior reports showing inconsistent dependencies on variables such as growth method and high energy particle irradiation conditions.[7,37,45,47,49,50]

This is the author's peer reviewed, accepted manuscript. However, the online version of record will be different from this version once it has been copyedited and typeset.
PLEASE CITE THIS ARTICLE AS DOI: 10.1063/5.0160541

AIP Publishing APL Materials ACCEPTED MANUSCRIPT

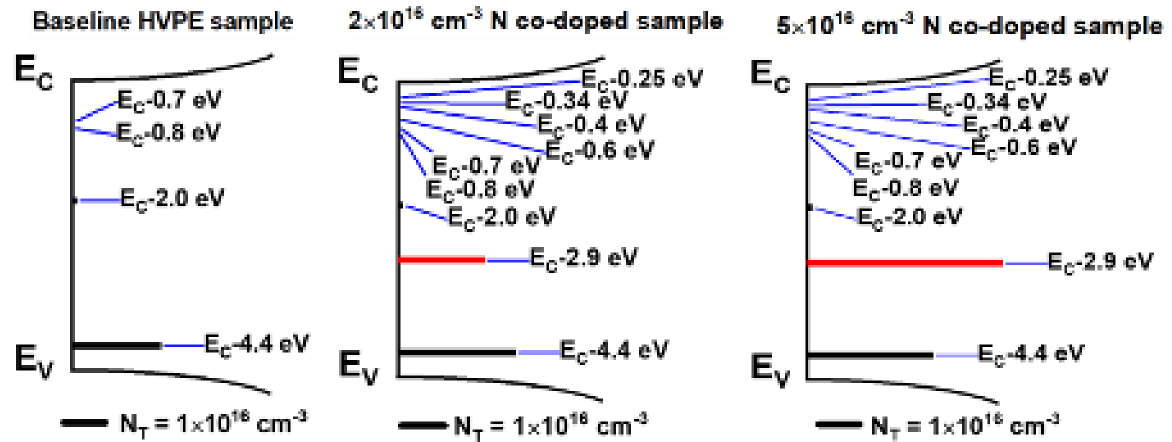

Figure 5: Summary of the energy positions and concentrations for traps detected by DLTS and DLOS in baseline HVPE, 2×10^{16} cm^{-3}, and 5×10^{16} cm^{-3} N co-doped HVPE samples. The lambda-corrected DLTS-detected trap concentrations are in the upper 1 eV from the conduction band, while the DLOS-detected trap concentrations are measured from LCV. E_C-2.9 eV trap concentration measured from LCV tracks with an increase in nitrogen implant concentration highlighted in red color.

The above experimental studies strongly indicate the E_C-2.9 eV state is due to a nitrogen acceptor. To provide further verification and confirm the charge state and the possible physical defect configuration causing the emission process, we performed DFT studies. The calculations used projector augmented wave potentials [51,52] as implemented in the VASP code.[53] Ga 3*d* electrons were treated as valence states. We used the Heyd–Scuseria–Ernzerhof (HSE) hybrid functional[54], with the screening parameter fixed at the standard value and the fraction of screened Hartree–Fock exchange set to 0.33, resulting in a direct bandgap of 4.9 eV. For nitrogen impurity calculations we employed 160-atom supercells, a plane-wave energy cutoff of 500 eV, and a single special k-point at (0.25, 0.25, 0.25). Energies of various configurations and charge states were calculated using the formalism defined by Freysoldt *et al.*,[55] including charge-state corrections.[56–58]

As noted in Peelaers *et al.* [11] the $N_{O(III)}$ configuration has the lowest energy among the three possible substitutional oxygen sites when the Fermi level is above 3 eV, a condition that is fulfilled in these Si-doped samples. As noted in the introduction, the (0/-) charge-state transition levels for the nitrogen impurity were found to strongly depend on the site on which the nitrogen atom substitutes; again, it is the level for $N_{O(III)}$, at E_C-2.84 eV, that closely matches the trap energy extracted from optical cross-section shown in Fig. 6(a). In order to further confirm this identification, we calculated configuration coordinate diagrams[59] in the one-dimensional approximation, which works very well when electron-phonon coupling is very strong as is clearly the case here. The diagram in Fig. 6(b) illustrates the potential energy surfaces as a function of atomic coordinates for the $N_{O(III)}$ impurity in the (ground-state, g) negative and (excited-state, e) neutral charge state, showing a large change in configuration coordinate ΔQ. The zero-phonon line (ZPL) energy E_{ZPL} corresponds to the charge-state transition level with respect to the conduction-band minimum, and effective phonon frequencies for ground and excited states are

indicated. Within this model, the Franck–Condon (D_{FC}) energy for the excitation process is the difference between the peak absorption energy E_{abs} and E_{ZPL}, and thus given by 4.15-2.84=1.31 eV, in very good agreement with the D_{FC} value extracted from the Pässler model shown in Fig 6a.

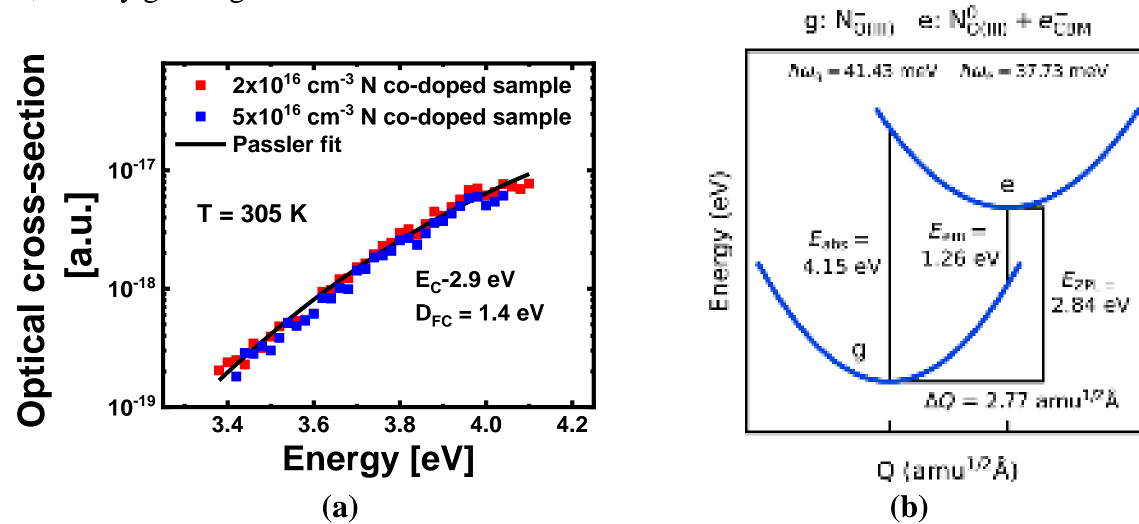

Figure 6 (a): The optical cross-section extracted from the photocapacitance transients of the N co-doped samples fitted to a Pässler model[43] for calculating the equilibrium trap energy and D_{FC}. E_C-2.9 eV shows similar N-concentration as implanted and has a large D_{FC} of 1.4 eV, implying broad lattice relaxation. **(b)** Configuration coordinate diagram calculated by DFT for $N_{O(III)}$ illustrating the optical transition that matches the optical cross-section fitting results.

In conclusion, this study investigates the use of N as a deep acceptor dopant in β-Ga_2O_3 through ion implantation. Strong evidence of background carrier compensation with implanted N is presented, demonstrating over 95% dopant activation under optimized conditions. This work establishes a clear correlation between the nitrogen implant concentration and the E_C-2.9 eV level determined by DLOS. As the nitrogen implantation concentration increases, there is a monotonic increase in the concentration of the E_C-2.9 eV level, resulting in effective carrier compensation. First-principles DFT calculations indicate a (0/-1) transition for this state, verifying its acceptor-like behavior and showing that the experimentally observed configuration is for nitrogen occupying O site III ($N_{O(III)}$), resulting in a deep compensating center at E_C-2.9 eV. Furthermore, the photoionization of the $N_{O(III)}$ acceptor is accompanied by a large local lattice relaxation, leading to a high Franck-Condon (D_{FC}) energy of 1.4 eV in the configuration coordinate diagram. This energy was experimentally obtained by analyzing the optical cross-section derived from DLOS. This combined experimental and theoretical effort shows that nitrogen doping is a very effective process to introduce extremely efficient deep acceptors for the purpose of achieving very high degrees of controlled carrier compensation in β-Ga_2O_3.

The authors acknowledge the funding support from the Air Force Office of Scientific Research No. FA9550-18-1-0479 (Ali Sayir, Program Manager) and from the US Air Force Radiation Effects Center of Excellence, Grant No. FA9550-22-1-0012. This work was supported in part by The Ohio State University Institute for Materials Research. This material is based on research sponsored by the Air Force Research Laboratory and Strategic Council for Higher Education under agreement FA8650-19-2-9300 and the Ohio Department of Higher Education and

AIP Publishing APL Materials ACCEPTED MANUSCRIPT
This is the author's peer reviewed, accepted manuscript. However, the online version of record will be different from this version once it has been copyedited and typeset.
PLEASE CITE THIS ARTICLE AS DOI: 10.1063/5.0160541

AIP Publishing APL Materials ACCEPTED MANUSCRIPT
This is the author's peer reviewed, accepted manuscript. However, the online version of record will be different from this version once it has been copyedited and typeset.
PLEASE CITE THIS ARTICLE AS DOI: 10.1063/5.0160541

Strategic Council for Higher Education under Ohio House Bill 49 of the 132nd General Assembly. The authors acknowledge the funding support from Department of Energy/National Nuclear Security Administration under Award Number(s) DE-NA0003921. This work was supported by the Air Force Office of Scientific Research (Grant No. FA9550-22-1-0165), the Research Council of Norway through the GO-POW project (Grant No. 314017), the University of Kansas General Research Fund allocation #2151089, the Office of Naval Research/NRL Basic Research Program, and partially performed under the auspices of the U.S. Department of Energy by Lawrence Livermore National Laboratory (LLNL) under Contract DE-AC52-07NA27344. The computations were performed on resources provided by UNINETT Sigma2 the National Infrastructure for High Performance Computing and Data Storage in Norway, and by the Extreme Science and Engineering Discovery Environment (XSEDE), supported by the National Science Foundation (Grant No. ACI-1548562). This work was supported by Air Force Office of Scientific Research No. FA9550-18-1-0479 and National Science Foundation Award Nos. ECCS 2019749 and ECCS 2231026. Any opinions, findings, conclusions, or recommendations expressed in this material are those of the authors and do not necessarily reflect the views of the funding provider.

REFERENCES:

[1] H.H. Tippins, "Optical Absorption and Photoconductivity in the Band Edge of β − Ga 2 O 3," Phys. Rev. **140**(1A), A316–A319 (1965).

[2] M. Orita, H. Ohta, M. Hirano, and H. Hosono, "Deep-ultraviolet transparent conductive β-Ga2O3 thin films," Appl. Phys. Lett. **77**(25), 4166–4168 (2000).

[3] T. Onuma, S. Saito, K. Sasaki, T. Masui, T. Yamaguchi, T. Honda, and M. Higashiwaki, "Valence band ordering in β-Ga $_2$ O $_3$ studied by polarized transmittance and reflectance spectroscopy," Jpn. J. Appl. Phys. **54**(11), 112601 (2015).

[4] M.J. Tadjer, J.L. Lyons, N. Nepal, J.A. Freitas, A.D. Koehler, and G.M. Foster, "Editors' Choice—Review—Theory and Characterization of Doping and Defects in β-Ga $_2$ O $_3$," ECS J. Solid State Sci. Technol. **8**(7), Q3187–Q3194 (2019).

[5] S.J. Pearton, J. Yang, P.H. Cary, F. Ren, J. Kim, M.J. Tadjer, and M.A. Mastro, "A review of Ga $_2$ O $_3$ materials, processing, and devices," Appl. Phys. Rev. **5**(1), 011301 (2018).

[6] H.J. Ghadi, J.F. McGlone, E. Farzana, A.R. Arehart, and S.A. Ringel, in *Ultrawide Bandgap B-Ga2O3 Semicond. Theory Appl.*, edited by J.S. Speck and E. Farzana (AIP Publishing LLC, n.d.), p. 0.

[7] J.F. McGlone, H. Ghadi, E. Cornuelle, A. Armstrong, G. Burns, Z. Feng, A.F.M.A. Uddin Bhuiyan, H. Zhao, A.R. Arehart, and S.A. Ringel, "Proton radiation effects on electronic defect states in MOCVD-grown (010) *β* -Ga $_2$ O $_3$," J. Appl. Phys. **133**(4), 045702 (2023).

[8] Z. Xia, H. Xue, C. Joishi, J. Mcglone, N.K. Kalarickal, S.H. Sohel, M. Brenner, A. Arehart, S. Ringel, S. Lodha, W. Lu, and S. Rajan, "β -Ga2O3 Delta-Doped Field-Effect Transistors With Current Gain Cutoff Frequency of 27 GHz," IEEE Electron Device Lett. **40**(7), 1052–1055 (2019).

[9] Y. Zhang, Z. Xia, C. Joishi, and S. Rajan, in *2018 76th Device Res. Conf. DRC* (2018), pp. 1–2.

[10] K.D. Chabak, J.P. McCandless, N.A. Moser, A.J. Green, K. Mahalingam, A. Crespo, N. Hendricks, B.M. Howe, S.E. Tetlak, K. Leedy, R.C. Fitch, D. Wakimoto, K. Sasaki, A. Kuramata, and G.H. Jessen, "Recessed-Gate Enhancement-Mode $\beta $ -Ga2O3 MOSFETs," IEEE Electron Device Lett. **39**(1), 67–70 (2018).

ACCEPTED MANUSCRIPT
APL Materials
AIP Publishing
This is the author's peer reviewed, accepted manuscript. However, the online version of record will be different from this version once it has been copyedited and typeset.
PLEASE CITE THIS ARTICLE AS DOI: 10.1063/5.0160541

[11] H. Peelaers, J.L. Lyons, J.B. Varley, and C.G. Van de Walle, "Deep acceptors and their diffusion in Ga_2O_3," APL Mater. **7**(2), 022519 (2019).
[12] M.E. Ingebrigtsen, J.B. Varley, A.Yu. Kuznetsov, B.G. Svensson, G. Alfieri, A. Mihaila, U. Badstübner, and L. Vines, "Iron and intrinsic deep level states in Ga_2O_3," Appl. Phys. Lett. **112**(4), 042104 (2018).
[13] P. Seyidov, J.B. Varley, Z. Galazka, T.-S. Chou, A. Popp, A. Fiedler, and K. Irmscher, "Cobalt as a promising dopant for producing semi-insulating β-Ga_2O_3 crystals: Charge state transition levels from experiment and theory," APL Mater. **10**(11), 111109 (2022).
[14] J.L. Lyons, "A survey of acceptor dopants for β-Ga2O3," Semicond. Sci. Technol. **33**(5), 05LT02 (2018).
[15] K. Irmscher, Z. Galazka, M. Pietsch, R. Uecker, and R. Fornari, "Electrical properties of β-Ga_2O_3 single crystals grown by the Czochralski method," J. Appl. Phys. **110**(6), 063720 (2011).
[16] Z. Galazka, R. Uecker, K. Irmscher, M. Albrecht, D. Klimm, M. Pietsch, M. Brützam, R. Bertram, S. Ganschow, and R. Fornari, "Czochralski growth and characterization of β-Ga2O3 single crystals," Cryst. Res. Technol. **45**(12), 1229–1236 (2010).
[17] N.T. Son, Q.D. Ho, K. Goto, H. Abe, T. Ohshima, B. Monemar, Y. Kumagai, T. Frauenheim, and P. Deák, "Electron paramagnetic resonance and theoretical study of gallium vacancy in β-Ga2O3," Appl. Phys. Lett. **117**(3), 032101 (2020).
[18] S. Bhandari, and M.E. Zvanut, "Charge trapping at Fe due to midgap levels in Ga_2O_3," J. Appl. Phys. **129**(8), 085703 (2021).
[19] J.F. McGlone, Z. Xia, C. Joishi, S. Lodha, S. Rajan, S. Ringel, and A.R. Arehart, "Identification of critical buffer traps in Si δ-doped β-Ga_2O_3 MESFETs," Appl. Phys. Lett. **115**(15), 153501 (2019).
[20] J.F. Mcglone, Z. Xia, Y. Zhang, C. Joishi, S. Lodha, S. Rajan, S.A. Ringel, and A.R. Arehart, "Trapping Effects in Si δ -Doped β -Ga2O3 MESFETs on an Fe-Doped β -Ga2O3 Substrate," IEEE Electron Device Lett. **39**(7), 1042–1045 (2018).
[21] H. Ghadi, J.F. McGlone, E. Cornuelle, Z. Feng, Y. Zhang, L. Meng, H. Zhao, A.R. Arehart, and S.A. Ringel, "Deep level defects in low-pressure chemical vapor deposition grown (010) β-Ga2O3," APL Mater. **10**(10), 101110 (2022).
[22] H. Gao, S. Muralidharan, N. Pronin, M.R. Karim, S.M. White, T. Asel, G. Foster, S. Krishnamoorthy, S. Rajan, L.R. Cao, M. Higashiwaki, H. von Wenckstern, M. Grundmann, H. Zhao, D.C. Look, and L.J. Brillson, "Optical signatures of deep level defects in Ga2O3," Appl. Phys. Lett. **112**(24), 242102 (2018).
[23] I. Hany, G. Yang, C.E. Zhou, C. Sun, K. Gundogdu, D. Seyitliyev, E.O. Danilov, F.N. Castellano, D. Sun, and E. Vetter, "Low temperature cathodoluminescence study of Fe-doped β-Ga2O3," Mater. Lett. **257**, 126744 (2019).
[24] A. Mauze, Y. Zhang, T. Mates, F. Wu, and J.S. Speck, "Investigation of unintentional Fe incorporation in (010) β-Ga2O3 films grown by plasma-assisted molecular beam epitaxy," Appl. Phys. Lett. **115**(5), 052102 (2019).
[25] Z. Wen, K. Khan, X. Zhai, and E. Ahmadi, "Si doping of β-Ga2O3 by disilane via hybrid plasma-assisted molecular beam epitaxy," Appl. Phys. Lett. **122**(8), 082101 (2023).
[26] F. Alema, Y. Zhang, A. Osinsky, N. Valente, A. Mauze, T. Itoh, and J.S. Speck, "Low temperature electron mobility exceeding 10^4 cm^2/V s in MOCVD grown **β**-Ga_2O_3," APL Mater. **7**(12), 121110 (2019).

AIP Publishing APL Materials ACCEPTED MANUSCRIPT
This is the author's peer reviewed, accepted manuscript. However, the online version of record will be different from this version once it has been copyedited and typeset.
PLEASE CITE THIS ARTICLE AS DOI: 10.1063/5.0160541

[27] A.Y. Polyakov, N.B. Smirnov, I.V. Shchemerov, S.J. Pearton, F. Ren, A.V. Chernykh, and A.I. Kochkova, "Electrical properties of bulk semi-insulating β-Ga_2O_3 (Fe)," Appl. Phys. Lett. **113**(14), 142102 (2018).
[28] J.F. Mcglone, Z. Xia, Y. Zhang, C. Joishi, S. Lodha, S. Rajan, S.A. Ringel, and A.R. Arehart, "Trapping Effects in Siδ-Dopedβ-Ga2O3MESFETs on an Fe-Dopedβ-Ga2O3Substrate," IEEE Electron Device Lett. **39**(7), 1042–1045 (2018).
[29] Q.D. Ho, T. Frauenheim, and P. Deák, "Theoretical confirmation of the polaron model for the Mg acceptor in β-Ga_2O_3," J. Appl. Phys. **124**(14), 145702 (2018).
[30] M.H. Wong, C.-H. Lin, A. Kuramata, S. Yamakoshi, H. Murakami, Y. Kumagai, and M. Higashiwaki, "Acceptor doping of β-Ga_2O_3 by Mg and N ion implantations," Appl. Phys. Lett. **113**(10), 102103 (2018).
[31] C. De Santi, M. Fregolent, M. Buffolo, M.H. Wong, M. Higashiwaki, G. Meneghesso, E. Zanoni, and M. Meneghini, "Carrier capture kinetics, deep levels, and isolation properties of β-Ga_2O_3 Schottky-barrier diodes damaged by nitrogen implantation," Appl. Phys. Lett. **117**(26), 262108 (2020).
[32] F. Alema, Y. Zhang, A. Osinsky, N. Orishchin, N. Valente, A. Mauze, and J.S. Speck, "Low 1014 cm−3 free carrier concentration in epitaxial β-Ga_2O_3 grown by MOCVD," APL Mater. **8**(2), 021110 (2020).
[33] K. Nomura, K. Goto, R. Togashi, H. Murakami, Y. Kumagai, A. Kuramata, S. Yamakoshi, and A. Koukitu, "Thermodynamic study of β-Ga2O3 growth by halide vapor phase epitaxy," J. Cryst. Growth **405**, 19–22 (2014).
[34] A. Kuramata, K. Koshi, S. Watanabe, Y. Yamaoka, T. Masui, and S. Yamakoshi, "High-quality β-Ga2O3 single crystals grown by edge-defined film-fed growth," Jpn. J. Appl. Phys. **55**(12), 1202A2 (2016).
[35] J.F. Ziegler, M.D. Ziegler, and J.P. Biersack, "SRIM - The stopping and range of ions in matter (2010)," Nucl. Instrum. Methods Phys. Res. B **268**, 1818–1823 (2010).
[36] H. Ghadi, J.F. McGlone, C.M. Jackson, E. Farzana, Z. Feng, A.F.M.A.U. Bhuiyan, H. Zhao, A.R. Arehart, and S.A. Ringel, "Full bandgap defect state characterization of β-Ga_2O_3 grown by metal organic chemical vapor deposition," APL Mater. **8**(2), 021111 (2020).
[37] H. Ghadi, J.F. McGlone, Z. Feng, and S.A. Ringel, "Influence of growth temperature on defect states throughout the bandgap of MOCVD-grown β-Ga2O3," Appl. Phys. Lett., 7 (2020).
[38] Z. Zhang, E. Farzana, A.R. Arehart, and S.A. Ringel, "Deep level defects throughout the bandgap of (010) β-Ga_2O_3 detected by optically and thermally stimulated defect spectroscopy," Appl. Phys. Lett. **108**(5), 052105 (2016).
[39] H. Ghadi, J.F. McGlone, Z. Feng, A.F.M.A.U. Bhuiyan, Y. Zhang, H. Zhao, A. Armstrong, G.R. Burns, G. Vizkelethy, E. Bielejec, A.R. Arehart, and S.A. Ringel, in *Oxide-Based Mater. Devices XII* (SPIE, 2021), pp. 31–37.
[40] P. Blood, and J.W. Orton, *The Electrical Characterization of Semiconductors: Majority Carriers and Electron States* (Academic Press Limited, San Diego, CA, 1992).
[41] D.V. Lang, "Deep-level transient spectroscopy: A new method to characterize traps in semiconductors," J. Appl. Phys. **45**(7), 3023–3032 (1974).
[42] A. Chantre, G. Vincent, and D. Bois, "Deep-level optical spectroscopy in GaAs," Phys. Rev. B **23**(10), 5335–5359 (1981).
[43] R. Pässler, "Photoionization cross-section analysis for a deep trap contributing to current collapse in GaN field-effect transistors," J. Appl. Phys. **96**(1), 715–722 (2004).

AIP Publishing APL Materials ACCEPTED MANUSCRIPT
This is the author's peer reviewed, accepted manuscript. However, the online version of record will be different from this version once it has been copyedited and typeset.
PLEASE CITE THIS ARTICLE AS DOI: 10.1063/5.0160541

[44] A. Armstrong, A.R. Arehart, and S.A. Ringel, "A method to determine deep level profiles in highly compensated, wide band gap semiconductors," J. Appl. Phys. **97**(8), 083529 (2005).
[45] A.M. Armstrong, M.H. Crawford, A. Jayawardena, A. Ahyi, and S. Dhar, "Role of self-trapped holes in the photoconductive gain of β-gallium oxide Schottky diodes," J Appl Phys, 7 (2016).
[46] M.E. Ingebrigtsen, A.Yu. Kuznetsov, B.G. Svensson, G. Alfieri, A. Mihaila, U. Badstübner, A. Perron, L. Vines, and J.B. Varley, "Impact of proton irradiation on conductivity and deep level defects in β-Ga $_2$ O $_3$," APL Mater. **7**(2), 022510 (2019).
[47] H.J. Ghadi, J.F. McGlone, E. Farzana, A.R. Arehart, and S.A. Ringel, "Radiation Effects on β-Ga2O3 Materials and Devices," (2023).
[48] J.M. Johnson, Z. Chen, J.B. Varley, C.M. Jackson, E. Farzana, Z. Zhang, A.R. Arehart, H.-L. Huang, A. Genc, S.A. Ringel, C.G. Van de Walle, D.A. Muller, and J. Hwang, "Unusual Formation of Point-Defect Complexes in the Ultrawide-Band-Gap Semiconductor β − Ga 2 O 3," Phys. Rev. X **9**(4), 041027 (2019).
[49] E. Farzana, A. Mauze, J.B. Varley, T.E. Blue, J.S. Speck, A.R. Arehart, and S.A. Ringel, "Influence of neutron irradiation on deep levels in Ge-doped (010) β-Ga $_2$ O $_3$ layers grown by plasma-assisted molecular beam epitaxy," APL Mater. **7**(12), 121102 (2019).
[50] E. Farzana, M.F. Chaiken, T.E. Blue, A.R. Arehart, and S.A. Ringel, "Impact of deep level defects induced by high energy neutron radiation in β-Ga $_2$ O $_3$," APL Mater. **7**(2), 022502 (2019).
[51] P.E. Blöchl, "Projector augmented-wave method," Phys. Rev. B **50**(24), 17953–17979 (1994).
[52] G. Kresse, and D. Joubert, "From ultrasoft pseudopotentials to the projector augmented-wave method," Phys. Rev. B **59**(3), 1758–1775 (1999).
[53] G. Kresse, and J. Furthmüller, "Efficient iterative schemes for ab initio total-energy calculations using a plane-wave basis set," Phys. Rev. B **54**(16), 11169–11186 (1996).
[54] A.V. Krukau, O.A. Vydrov, A.F. Izmaylov, and G.E. Scuseria, "Influence of the exchange screening parameter on the performance of screened hybrid functionals," J. Chem. Phys. **125**(22), 224106 (2006).
[55] C. Freysoldt, B. Grabowski, T. Hickel, J. Neugebauer, G. Kresse, A. Janotti, and C.G. Van de Walle, "First-principles calculations for point defects in solids," Rev. Mod. Phys. **86**(1), 253–305 (2014).
[56] C. Freysoldt, J. Neugebauer, and C.G. Van de Walle, "Fully Ab Initio Finite-Size Corrections for Charged-Defect Supercell Calculations," Phys. Rev. Lett. **102**(1), 016402 (2009).
[57] Y. Kumagai, and F. Oba, "Electrostatics-based finite-size corrections for first-principles point defect calculations," Phys. Rev. B **89**(19), 195205 (2014).
[58] T. Gake, Y. Kumagai, C. Freysoldt, and F. Oba, "Finite-size corrections for defect-involving vertical transitions in supercell calculations," Phys. Rev. B **101**(2), 020102 (2020).
[59] A. Alkauskas, J.L. Lyons, D. Steiauf, and C.G. Van de Walle, "First-Principles Calculations of Luminescence Spectrum Line Shapes for Defects in Semiconductors: The Example of GaN and ZnO," Phys. Rev. Lett. **109**(26), 267401 (2012).

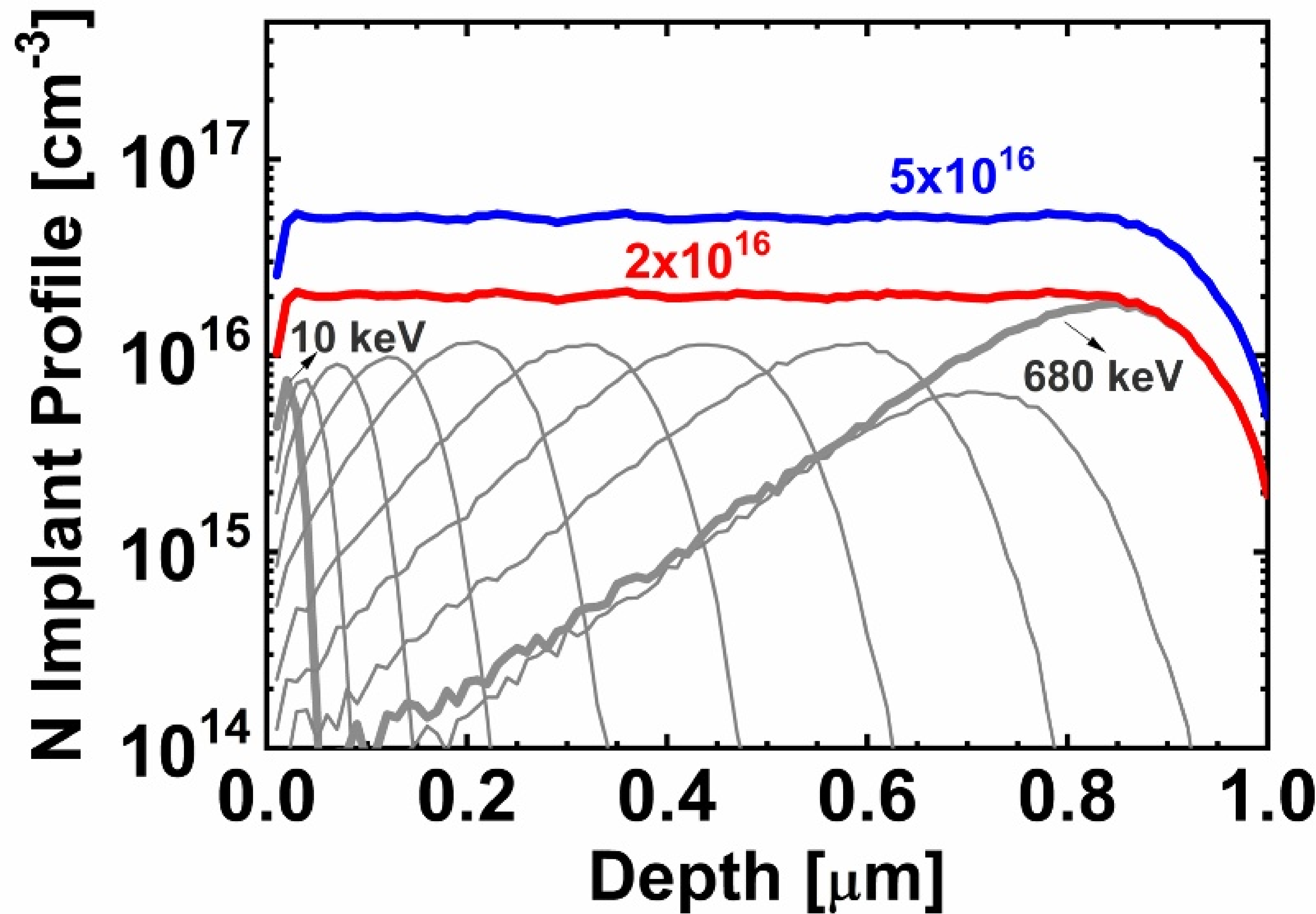

N Implant Profile [cm-3]
Depth [μm]
5x10^16
2x10^16
10 keV
680 keV
10^17
10^16
10^15
10^14
0.0
0.2
0.4
0.6
0.8
1.0

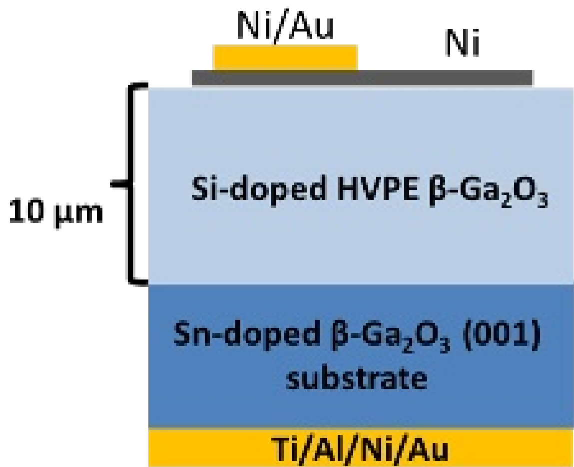
Ni/Au
Ni
10 μm
Si-doped HVPE β-Ga_2O_3
Sn-doped β-Ga_2O_3 (001)
substrate
Ti/Al/Ni/Au

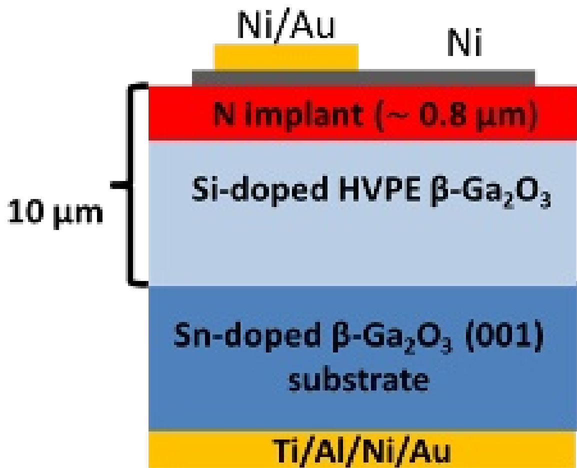
Ni/Au
Ni
N implant (~ 0.8 μm)
Si-doped HVPE β-Ga2O3
10 μm
Sn-doped β-Ga2O3 (001)
substrate
Ti/Al/Ni/Au

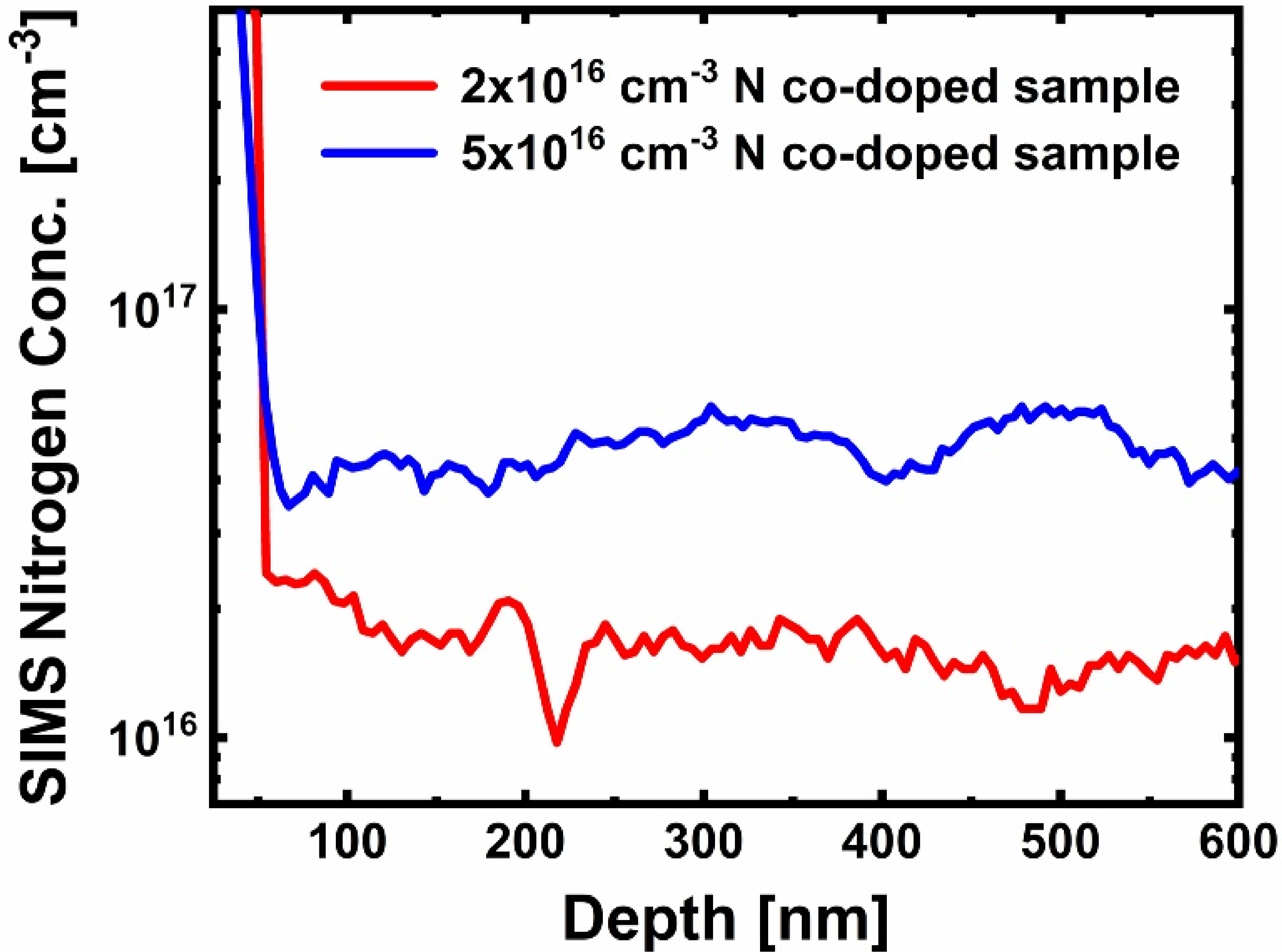
2x10^16 cm^-3 N co-doped sample
5x10^16 cm^-3 N co-doped sample
SIMS Nitrogen Conc. [cm^-3]
10^17
10^16
100
200
300
400
500
600
Depth [nm]

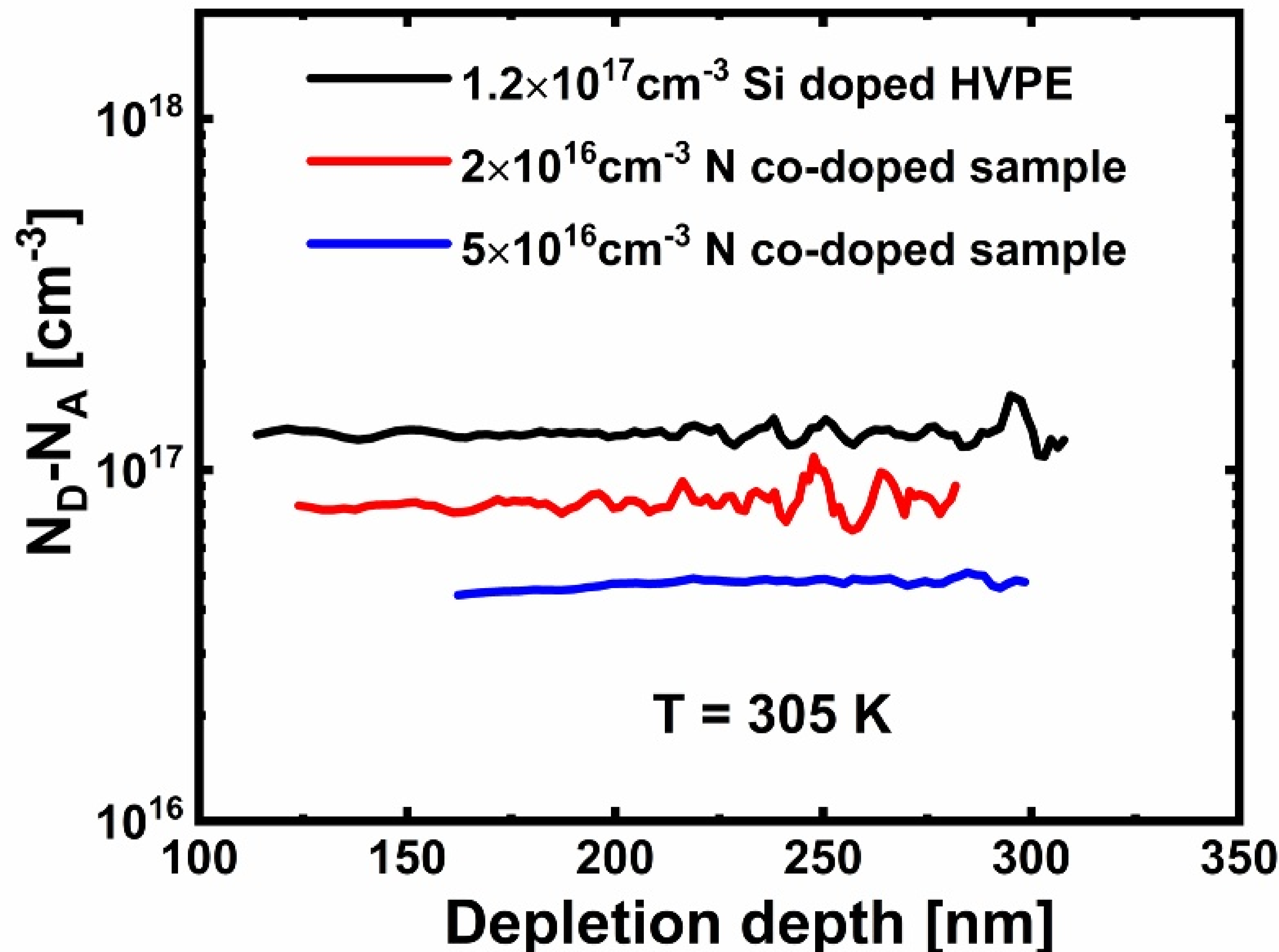

1.2×10^17cm^-3 Si doped HVPE
2×10^16cm^-3 N co-doped sample
5×10^16cm^-3 N co-doped sample
T = 305 K
10^18
10^17
10^16
N_D-N_A [cm^-3]
100
150
200
250
300
350
Depletion depth [nm]

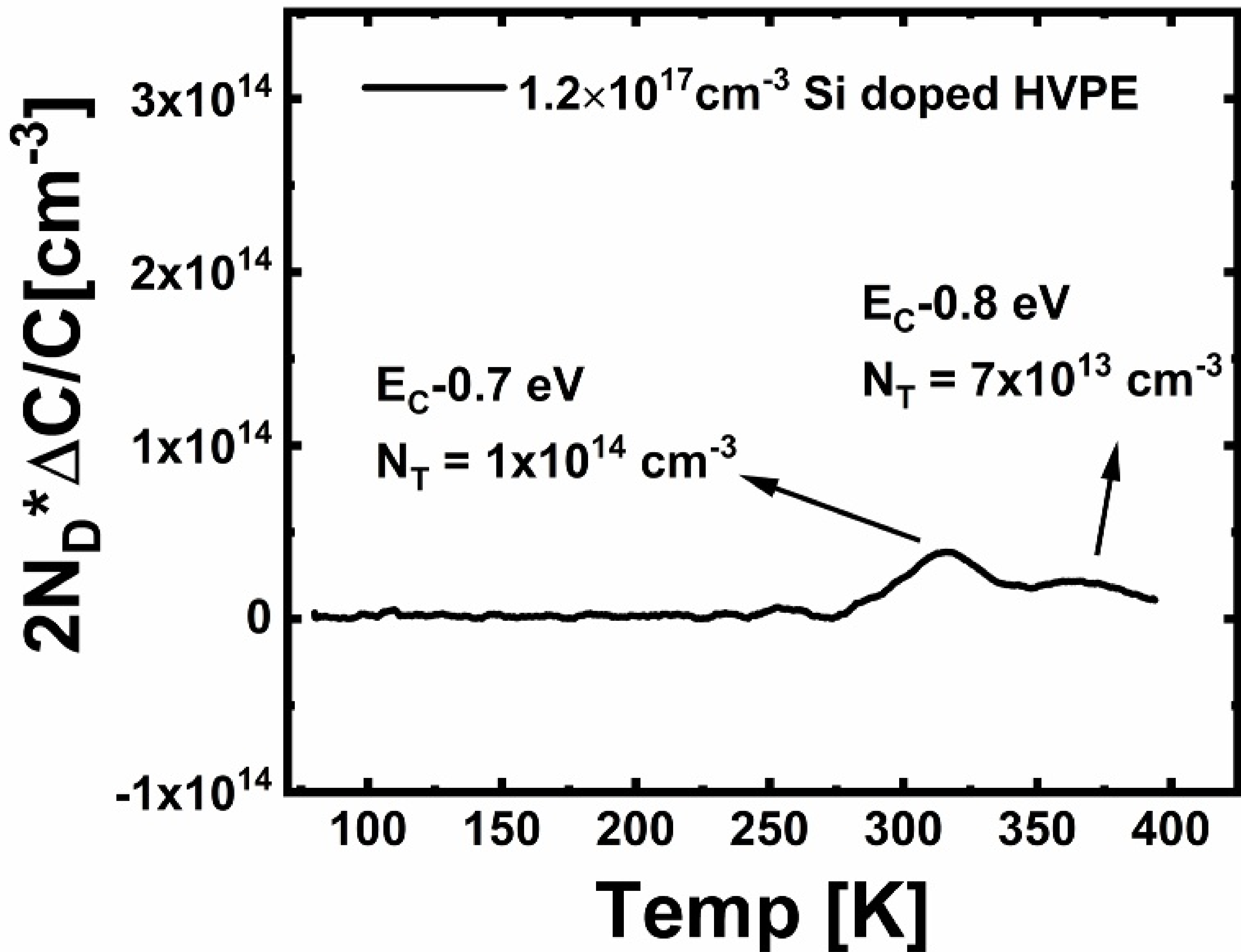

1.2×10^17cm^-3 Si doped HVPE
3x10^14
2x10^14
1x10^14
0
-1x10^14
2N_D*ΔC/C[cm^-3]
E_C-0.8 eV
N_T = 7x10^13 cm^-3
E_C-0.7 eV
N_T = 1x10^14 cm^-3
100
150
200
250
300
350
400
Temp [K]

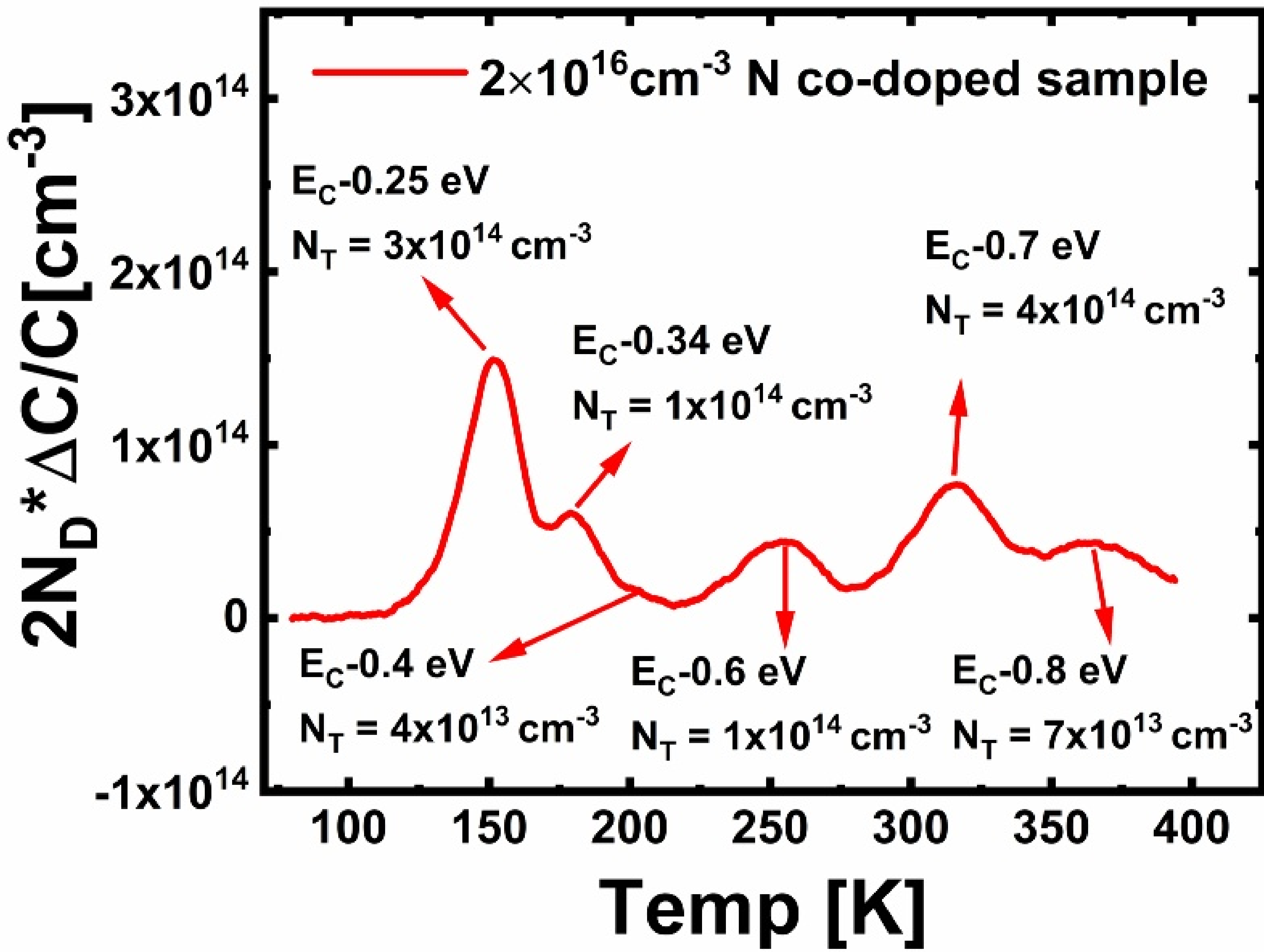

2×10^16 cm^-3 N co-doped sample
2N_D*ΔC/C[cm^-3]
3x10^14
2x10^14
1x10^14
0
-1x10^14
E_C-0.25 eV
N_T = 3x10^14 cm^-3
E_C-0.34 eV
N_T = 1x10^14 cm^-3
E_C-0.7 eV
N_T = 4x10^14 cm^-3
E_C-0.4 eV
N_T = 4x10^13 cm^-3
E_C-0.6 eV
N_T = 1x10^14 cm^-3
E_C-0.8 eV
N_T = 7x10^13 cm^-3
100
150
200
250
300
350
400
Temp [K]

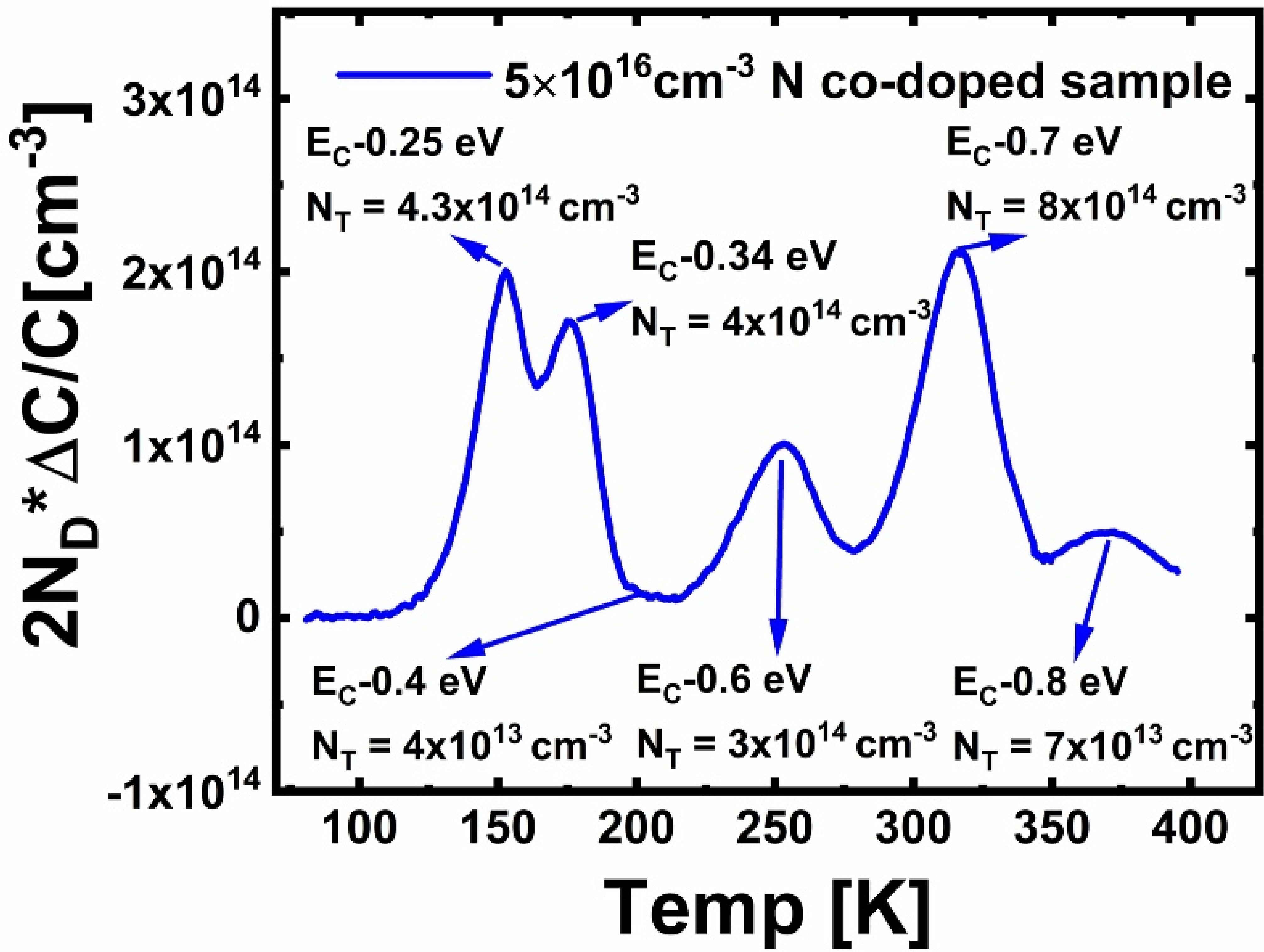
5×10^16cm^-3 N co-doped sample
3x10^14
2x10^14
1x10^14
0
-1x10^14
2N_D*ΔC/C[cm^-3]
E_C-0.25 eV
N_T = 4.3x10^14 cm^-3
E_C-0.34 eV
N_T = 4x10^14 cm^-3
E_C-0.7 eV
N_T = 8x10^14 cm^-3
E_C-0.4 eV
N_T = 4x10^13 cm^-3
E_C-0.6 eV
N_T = 3x10^14 cm^-3
E_C-0.8 eV
N_T = 7x10^13 cm^-3
100
150
200
250
300
350
400
Temp [K]

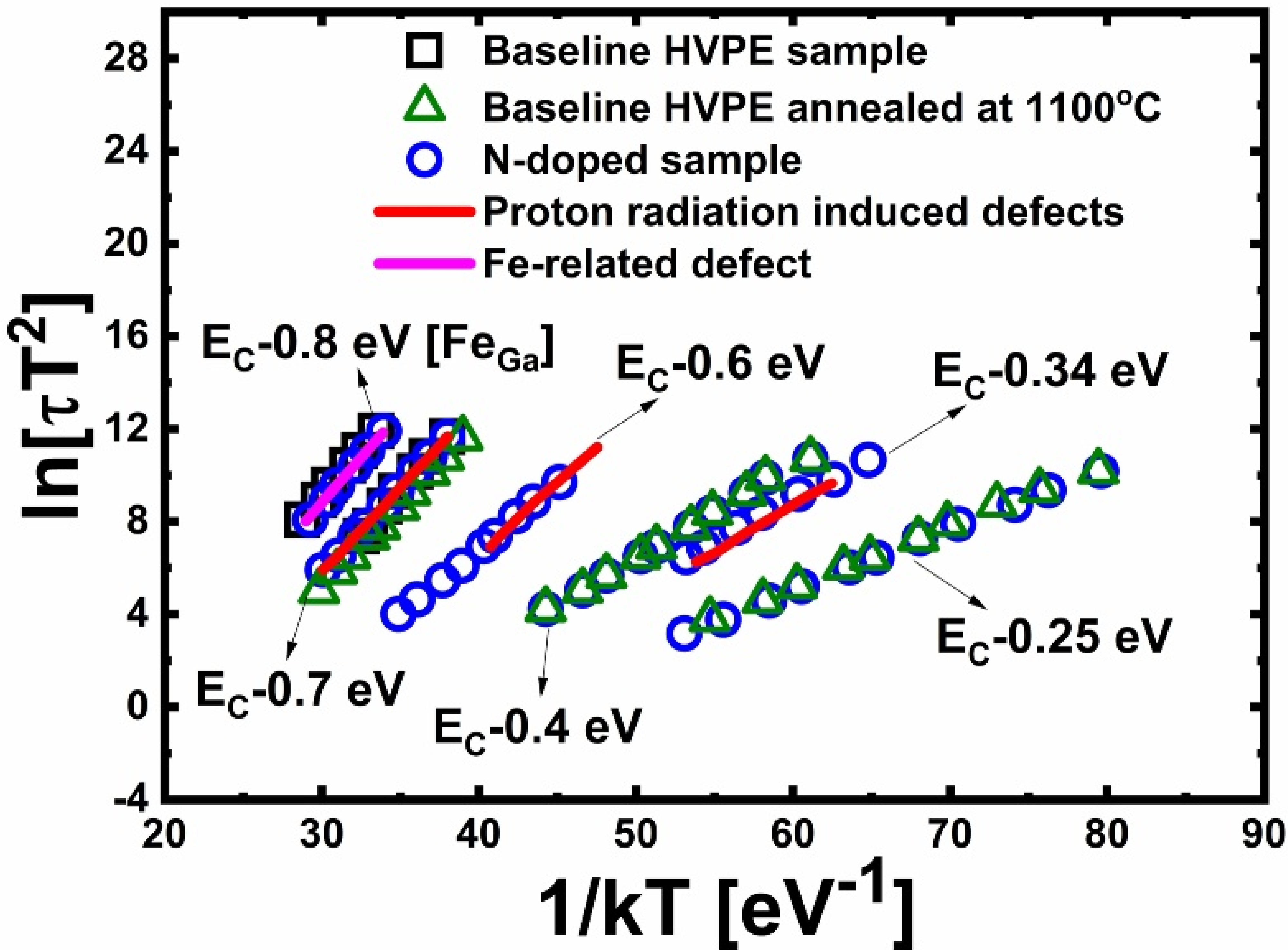

Baseline HVPE sample
Baseline HVPE annealed at 1100°C
N-doped sample
Proton radiation induced defects
Fe-related defect
E_C-0.8 eV [Fe_Ga]
E_C-0.6 eV
E_C-0.34 eV
E_C-0.7 eV
E_C-0.4 eV
E_C-0.25 eV
ln[τT^2]
1/kT [eV^-1]
28
24
20
16
12
8
4
0
-4
20
30
40
50
60
70
80
90

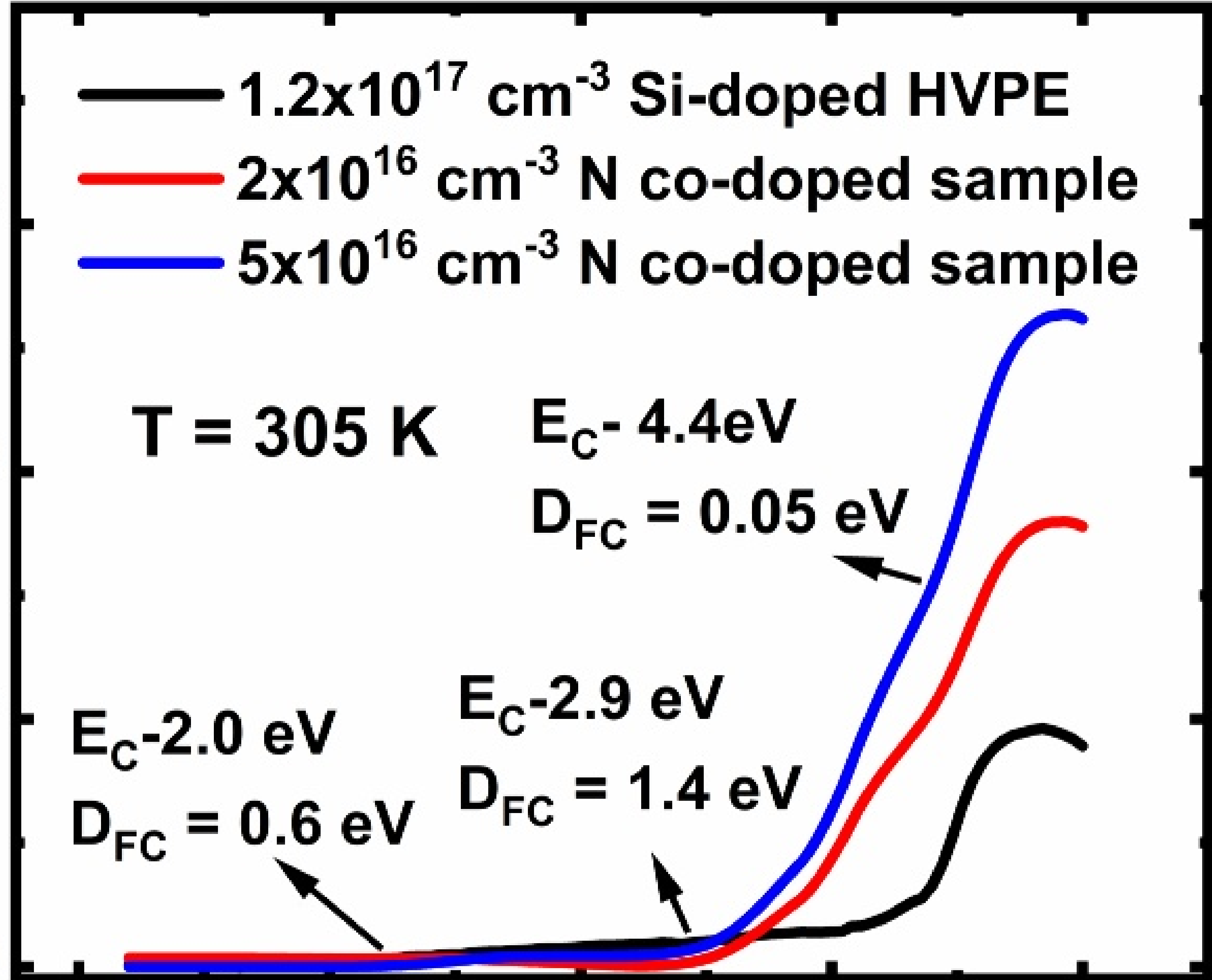

1.2x10^17 cm^-3 Si-doped HVPE
2x10^16 cm^-3 N co-doped sample
5x10^16 cm^-3 N co-doped sample
T = 305 K
E_C- 4.4eV
D_FC = 0.05 eV
E_C-2.9 eV
D_FC = 1.4 eV
E_C-2.0 eV
D_FC = 0.6 eV
2N_D*ΔC/C [cm^-3]
6.0x10^16
4.0x10^16
2.0x10^16
0.0
1
2
3
4
5
Energy [eV]

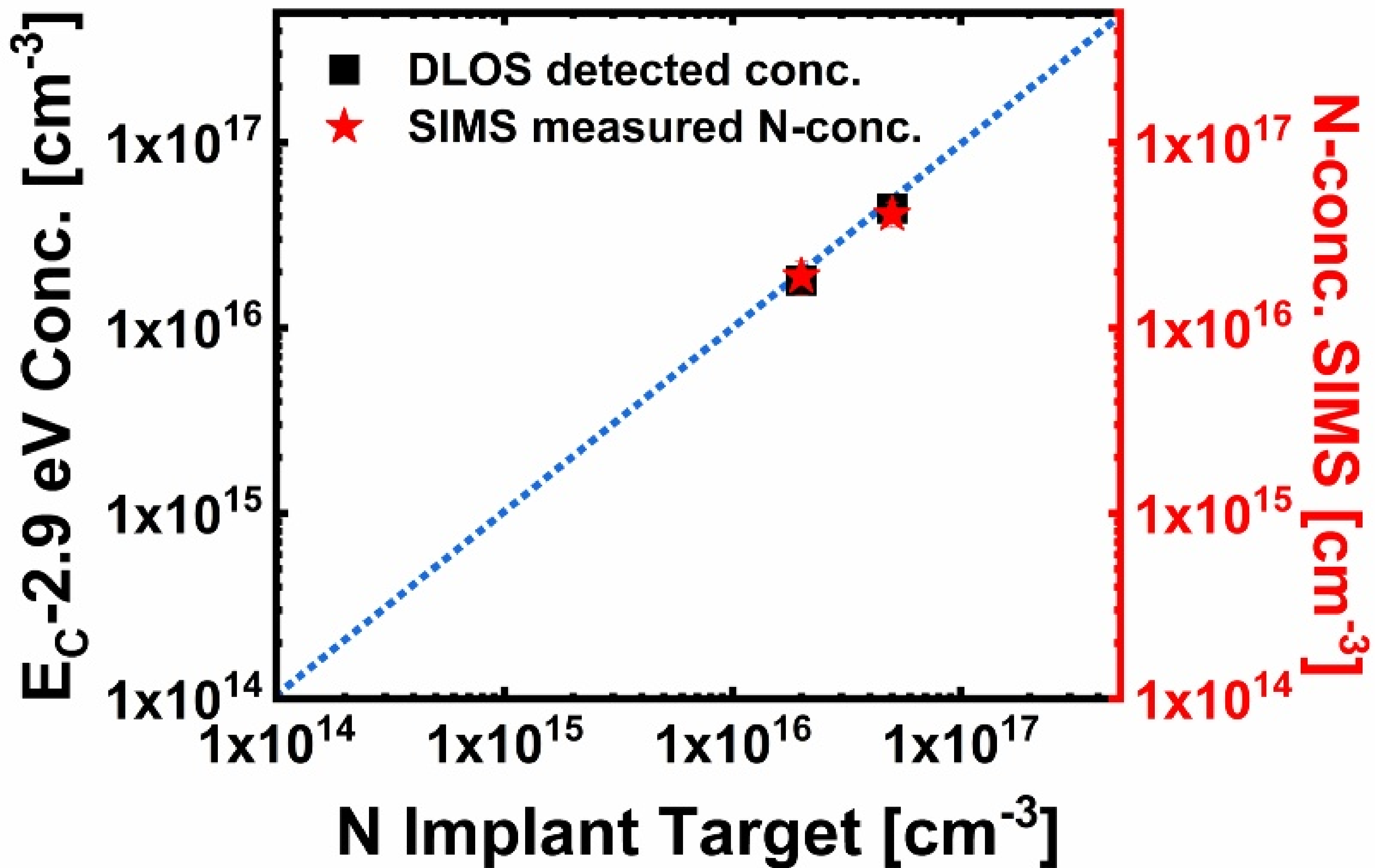

DLOS detected conc.
SIMS measured N-conc.
1x10^17
1x10^16
1x10^15
1x10^14
E_C-2.9 eV Conc. [cm^-3]
N-conc. SIMS [cm^-3]
N Implant Target [cm^-3]

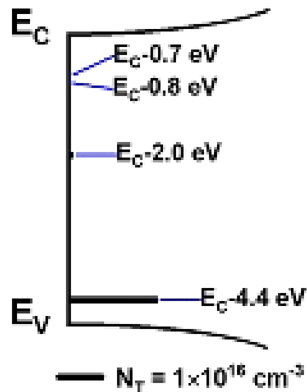
Baseline HVPE sample
E_C
E_C-0.7 eV
E_C-0.8 eV
E_C-2.0 eV
E_C-4.4 eV
E_V
$N_T = 1\times10^{16}$ cm^{-3}

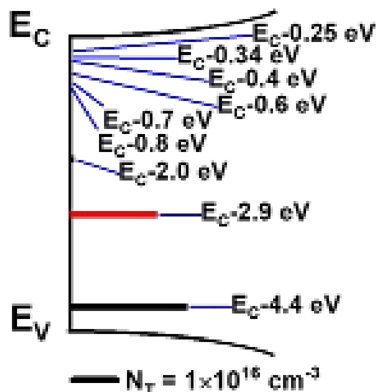
2×10^{16} cm^{-3} N co-doped sample
E_C
E_C-0.25 eV
E_C-0.34 eV
E_C-0.4 eV
E_C-0.6 eV
E_C-0.7 eV
E_C-0.8 eV
E_C-2.0 eV
E_C-2.9 eV
E_C-4.4 eV
E_V
$N_T = 1\times10^{16}$ cm^{-3}

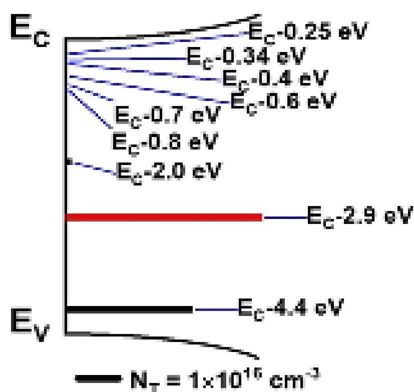
5×10^{16} cm^{-3} N co-doped sample
E_C
E_C-0.25 eV
E_C-0.34 eV
E_C-0.4 eV
E_C-0.6 eV
E_C-0.7 eV
E_C-0.8 eV
E_C-2.0 eV
E_C-2.9 eV
E_C-4.4 eV
E_V
$N_T = 1\times10^{16}$ cm^{-3}

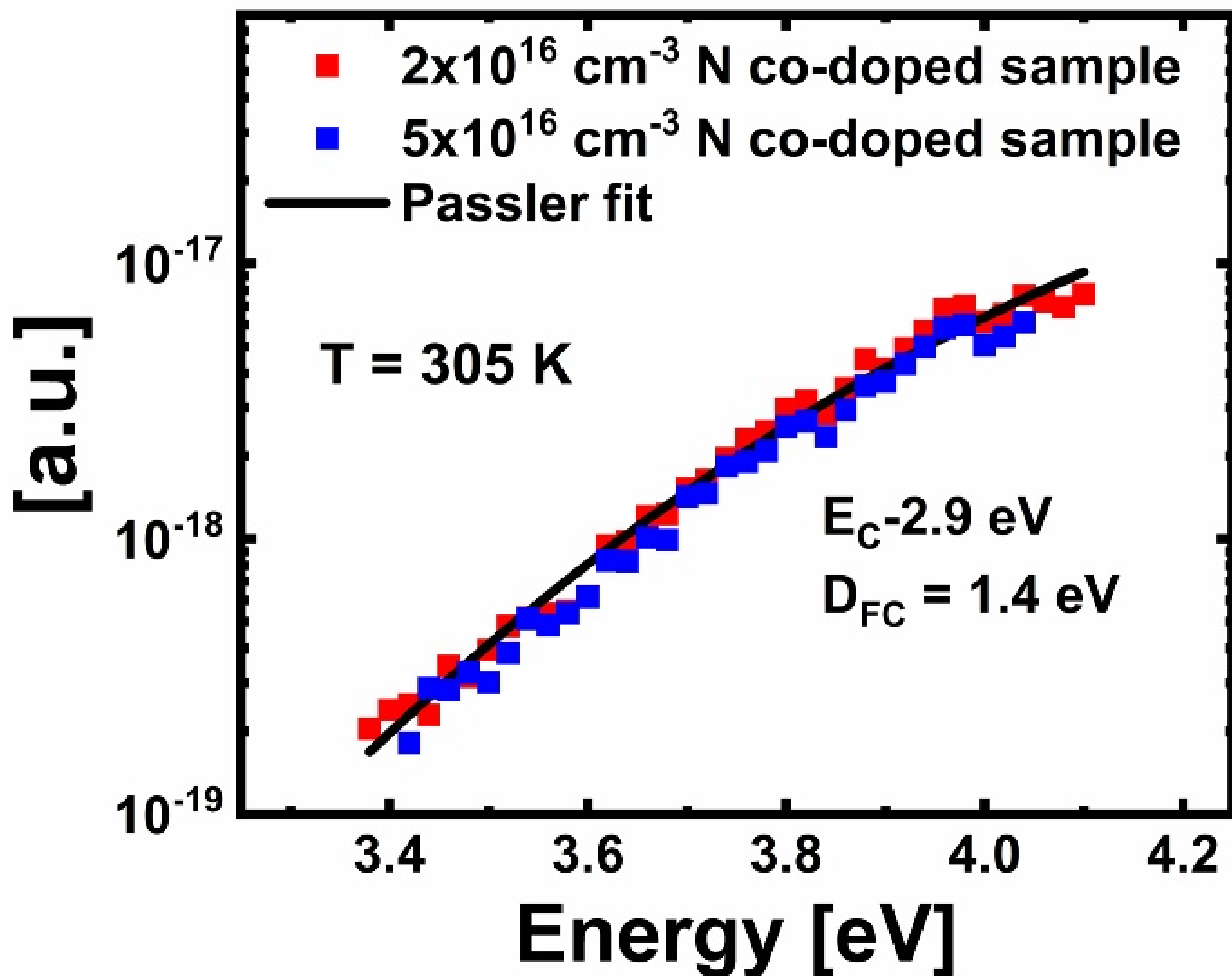

Optical cross-section [a.u.]
2x10^16 cm^-3 N co-doped sample
5x10^16 cm^-3 N co-doped sample
Passler fit
T = 305 K
E_C-2.9 eV
D_FC = 1.4 eV
10^-17
10^-18
10^-19
3.4
3.6
3.8
4.0
4.2
Energy [eV]

g: $N_{O(III)}^{-}$ e: $N_{O(III)}^{0} + e_{CBM}^{-}$
$\hbar\omega_g = 41.43$ meV
$\hbar\omega_e = 37.73$ meV
e
E_{abs} = 4.15 eV
E_{em} = 1.26 eV
E_{ZPL} = 2.84 eV
g
ΔQ = 2.77 amu$^{1/2}$Å
Energy (eV)
Q (amu$^{1/2}$Å)